ACS Chemical Neuroscience

pubs.acs.org/chemneuro Research Article

Development and Application of a Chemical Probe Based on a Neuroprotective Flavonoid Hybrid for Target Identification Using Activity-Based Protein Profiling

Sandra Gunesch, David Soriano-Castell, Stephanie Lamer, Andreas Schlosser, Pamela Maher,* and Michael Decker*

Cite This: https://dx.doi.org/10.1021/acschemneuro.0c00589 Read Online

ACCESS | Metrics & More | Article Recommendations | Supporting Information

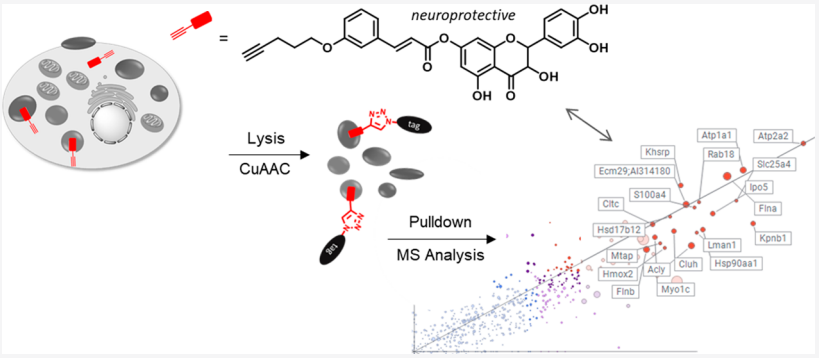

ABSTRACT: Alzheimer's disease (AD) is the most common form of dementia, and up to now, there are no disease-modifying drugs available. Natural product hybrids based on the flavonoid taxifolin and phenolic acids have shown a promising pleiotropic neuroprotective profile in cell culture assays and even disease-modifying effects *in vivo*. However, the detailed mechanisms of action remain unclear. To elucidate the distinct intracellular targets of 7-*O*-esters of taxifolin, we present in this work the development and application of a chemical probe, 7-*O*-cinnamoyltaxifolin-alkyne, for target identification using activity-based protein profiling. 7-*O*-Cinnamoyltaxifolin-alkyne remained neuroprotective in all cell culture assays. Western blot analysis showed a comparable influence on the same intracellular pathways as that of the lead compound 7-*O*-cinnamoyltaxifolin, thereby confirming its suitability as a probe for target identification experiments. Affinity pulldown and MS analysis revealed adenine nucleotide translocase 1 (ANT-1) and sarco/endoplasmic reticulum Ca^{2+} ATPase (SERCA) as intracellular interaction partners of 7-*O*-cinnamoyltaxifolin-alkyne and thus of 7-*O*-esters of taxifolin.

KEYWORDS: *Alzheimer's disease, natural product hybrids, CuAAC, neuroinflammation*

INTRODUCTION

Alzheimer's disease (AD) is the most common form of dementia and due to aging societies, the number of affected people is increasing dramatically.[1] AD is characterized by abnormal protein aggregation of hyperphosphorylated tau protein forming neurofibrillary tangles and amyloid β accumulation as extracellular plaques.[2] Neuroinflammation and oxidative stress are strong contributors to neurodegeneration and AD pathology.[3,4] Enhancing the pathophysiology of protein aggregation, oxidative stress and neuroinflammation may even represent key factors in AD development.[5] Currently, there are no disease-modifying drugs on the market. The only available treatments are symptomatic and cannot halt or cure the disease.[1] The complexity of AD and the lack of understanding of the details of its cause and progression are hampering drug development. It is important to broaden the knowledge about the molecular causes of the disease and focus on compounds with a pleiotropic neuroprotective profile to deal with the multifactorial nature of AD,[6] particularly as the one-target strategy has not been successful in drug discovery so far.[7]

Natural products have been used in traditional medicine and are gaining increased attention for their potential as neuroprotectants interfering with disease progression.[8−10] The well-established antioxidant features of natural products, i.e., their radical scavenging abilities, are important for neuroprotection

Received: September 8, 2020
Accepted: October 13, 2020

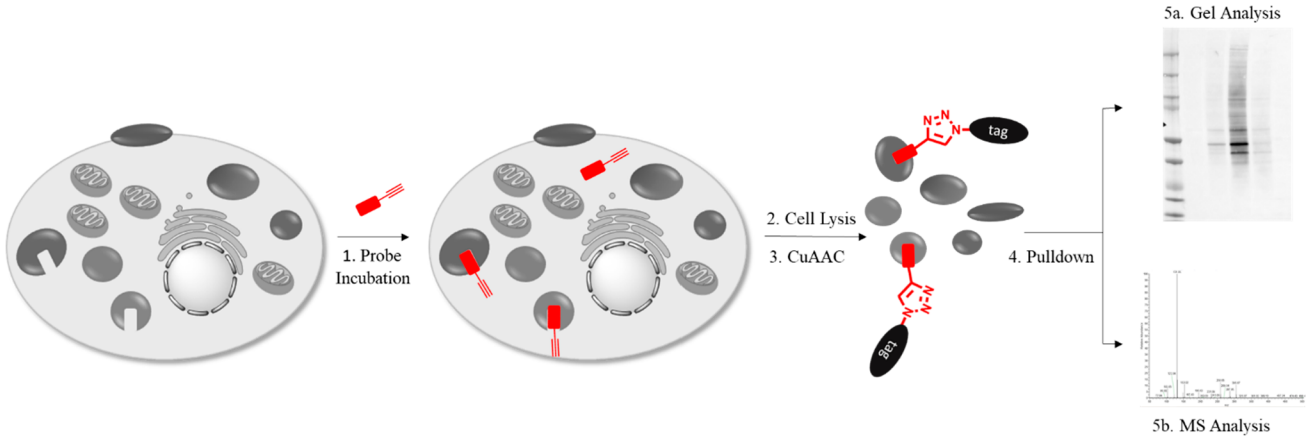

Figure 1. Workflow of the CuAAC approach for target identification. During incubation, the chemical probe binds to its native targets inside the cells. The cells are lysed and submitted to the CuAAC reaction to tag the chemical probe, which is covalently bound to its intracellular targets. After pulldown purification, target proteins are analyzed.

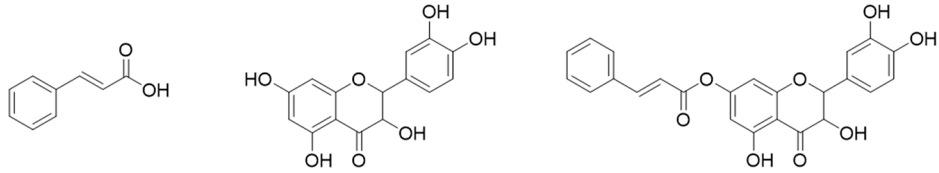

Figure 2. Chemical structures of cinnamic acid, the flavonoid taxifolin, and 7-*O*-cinnamoyltaxifolin (7CT).

induced by oxidative stress.[11] However, polyphenols as plant secondary metabolites have also shown to be neuroprotective by activating several intracellular pathways in addition to their antioxidative features.[12] The flavonoid fisetin, for example, was shown to activate the Ras-extracellular signal-regulated kinase (ERK) cascade and induced cAMP response element-binding protein (CREB) phosphorylation in rat hippocampal slices and therefore enhanced memory in mice.[13] Recently, it has been shown that the flavonoid taxifolin prevented neuroinflammation in a cerebral amyloid angiopathy mouse model by suppressing the ApoE-ERK1/2-amyloid-β precursor protein axis.[14] Phenolic acid esters of the flavonolignan silibinin are potent neuroprotectants and activate mouse microglia,[15] and esters of taxifolin upregulated the antioxidant response element (ARE) via nuclear factor (erythroid-derived 2)-like 2 (Nrf2) activation.[16,17] Even though the antioxidant and anti-inflammatory effects of these natural products are well-established and have been shown to translate into *in vivo* AD models where they ameliorated memory deficits,[13,17] the molecular mode of action and the exact intracellular targets of these compounds remain largely elusive.

To identify cellular targets of compounds, a bioorthogonal Cu(I)-catalyzed [3 + 2] azido-alkyne cycloaddition (CuAAC) approach can be used.[18−20] An alkyne tagged chemical probe of the compound of interest undergoes covalent interactions with its target proteins when incubated with cells (Figure 1). The alkyne probe binds to its native targets and can then be tagged with any azide in a CuAAC reaction. Depending on the application, tags can be fluorescent dyes or other markers for visualization and identification of target proteins. A widely used tag is biotin, as the high affinity for streptavidin is convenient for the enrichment of bound proteins and enables characterization by MS analysis.[19]

In our previous work, we showed that the 7-*O*-ester of the flavonoid taxifolin and cinnamic acid, namely, 7-*O*-cinnamoyltaxifolin (7CT), represented a highly neuroprotective compound acting in an overadditive manner (Figure 2).[17]

Specifically, at the concentrations tested, the individual components taxifolin and cinnamic acid or the equimolar mixture of both were not protective, whereas the ester hybrid 7-*O*-cinnamoyltaxifolin displayed pronounced neuroprotective activity. We observed the overadditive effect of 7-*O*-cinnamoyltaxifolin in a set of assays inducing protection against oxidative stress in neuronal HT22 cells but also investigating inhibition of inflammatory processes in BV-2 microglial cells.[17] Furthermore, the overadditive effect of 7-*O*-cinnamoyltaxifolin was translated to animals using an Aβ_{25-35}-induced memory-impaired AD mouse model where the compound was able to ameliorate short-term memory deficits.[17] The significant and overadditive effect *in vivo* of 7-*O*-cinnamoyltaxifolin showed that these natural product hybrids can be considered as a class of neuroprotective compounds with a distinct pharmacological profile. This is supported by structurally closely related 7-*O*-silibinin esters, which are sensitive to minor chemical modifications, indirectly ruling out unspecific effects underlying these properties.[15] However, to further develop the compound, it is indispensable to understand its mechanism of action and determine its intracellular targets.

The goal of this study was to design and synthesize a chemical probe of 7-*O*-cinnamoyltaxifolin suitable for target identification with the CuAAC approach. Previously, targets for xanthumol, a phytochemical of hops,[21] have been identified using this approach. Furthermore, a functional probe for flavonoid catabolites was developed by Nakashima et al. and used in the CuAAC reaction.[22] Here, we present 7-*O*-

https://dx.doi.org/10.1021/acschemneuro.0c00589
ACS Chem. Neurosci. XXXX, XXX, XXX−XXX

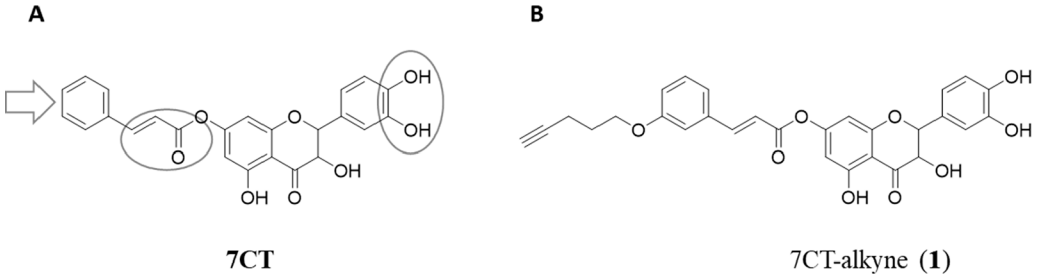

Figure 3. Chemical structures. (A) Design of the chemical probe without altering electrophilic moieties (encircled) of 7-*O*-cinnamoyltaxifolin. (B) The chemical structure of 7CT-alkyne (**1**).

Scheme 1. Synthesis of 7CT-Alkyne (1), a 7-*O*-Cinnamoyltaxifolin-Based Chemical Probe, and the Control Compound (2)[a]

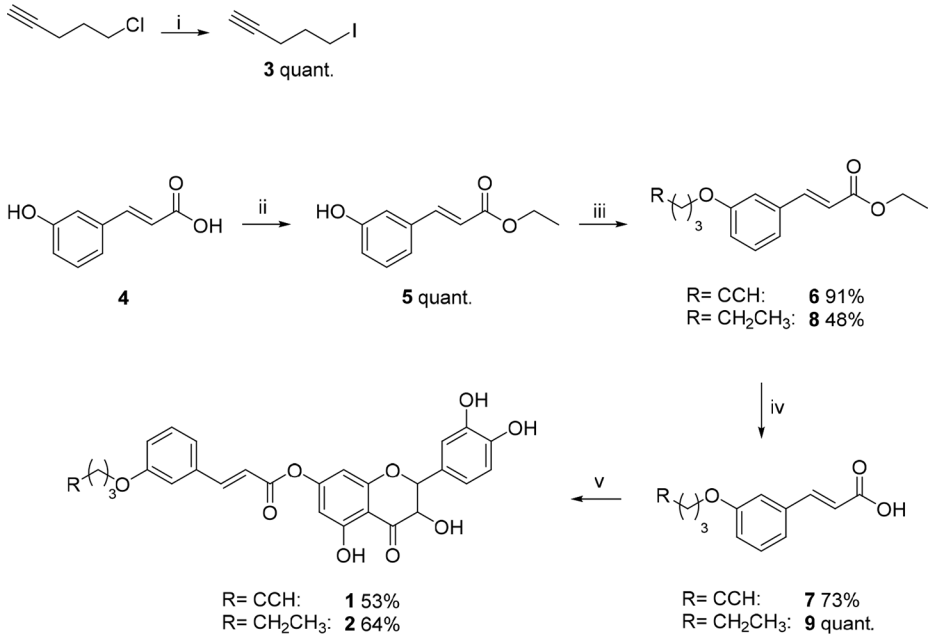

[a](i) NaI, dry acetone, reflux, overnight; (ii) H_2SO_4, ethanol, reflux, 6 h; (iii) **3**, K_2CO_3, dry acetone, 0 °C to reflux, overnight; (iv) NaOH, water, ethanol, room temperature; (v) (1) Oxalyl chloride, DMF, dry THF, rt, 30 min; (2) Taxifolin, triethylamine, rt, overnight.

cinnamoyltaxifolin-alkyne (7CT-alkyne, **1**, Figure 3B), a derivative of 7-*O*-cinnamoyltaxifolin (7CT), functioning as a chemical probe for intracellular target identification. Equivalent effects in relevant assays of neuroprotection and neuroinflammation of 7CT-alkyne **1** compared to those of 7CT proved the probes' interaction with the targets of the parent compound. Among others, ANT-1 and SERCA were identified as targets of **1** and 7CT.

RESULTS AND DISCUSSION

Aiming to identify intracellular targets of flavonoid esters and investigate their intracellular mode of neuroprotection, the chemical probe of 7-*O*-cinnamoyltaxifolin (7CT), compound **1**, was designed and synthesized to be used in a CuAAC reaction for affinity-based protein profiling. The suitability of **1** as a probe for 7CT was investigated in cell-based phenotypic screening assays and Western blots. Microscopic analysis of Cy3-coupled **1** suggested mitochondria as one of the subcellular locations of internalized **1**, which was supported by the identification of the mitochondrial ATP/ADP carrier ANT-1 in MS analysis of the pulldown.

Chemistry. It is of utmost importance not to alter the mode of action of the compound when designing a chemical probe for target identification purposes. For 7-*O*-cinnamoyltaxifolin, its simultaneous influence on several proteins and signaling pathways could be mediated through the Michael acceptor sites at the cinnamoyl moiety and the catechol residue, allowing covalent conjugation to proteins (Figure 3A). This is supported by comprehensive structure−activity relationship studies (SARs) on the respective silibinin ester.[15] The attack of a nucleophilic side chain, for example, of cysteinyl thiolates, to the electrophilic β-carbon could be one potential mechanism to form covalent adducts inducing cellular responses.[23] To preserve potential reactive sites in 7-*O*-cinnamoyltaxifolin, the aromatic moiety of the acid was chosen to introduce the alkyne tag necessary for CuAAC. In a previous SAR study with phenolic acid esters of silibinin[15] and also with 7-*O*-feruloyltaxifolin as a potent neuroprotectant,[17] we showed that this entity tolerates modification without loss of activity. Therefore, 7CT-alkyne (**1**) (Figure 3B) was synthesized starting from 3-hydroxy cinnamic acid (**4**). The carboxylic acid moiety was protected using ethanol to selectively react with 5-iodopentyne (**3**), which was synthesized via a Finkelstein reaction, at the aromatic hydroxyl position. Deprotection under basic conditions gave compound **7**. Regioselective esterification represents a considerable synthetic

https://dx.doi.org/10.1021/acschemneuro.0c00589
ACS Chem. Neurosci. XXXX, XXX, XXX−XXX

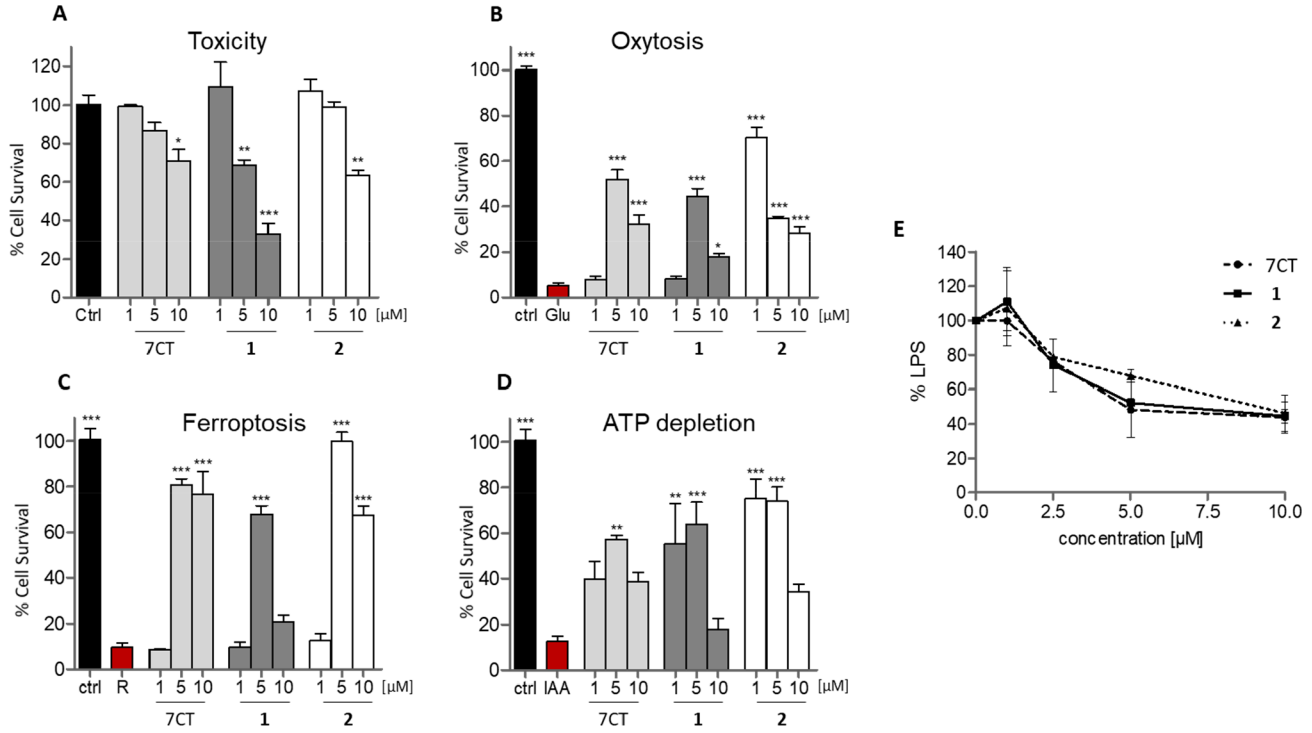

Figure 4. Phenotypic screening assays in HT22 hippocampal nerve cells and neuroinflammation in BV-2 cells. (A) Toxicity of the compounds 7CT, 7CT-alkyne (**1**), and 7CT-alkane (**2**). (B) Neuroprotective effects of 7CT, **1**, and **2** against oxytosis. Glutamate (5 mM) was used to induce toxicity (red). (C) Neuroprotection of 7CT, **1**, and **2** against ferroptosis induced by 0.3 μM RSL3 (red). (D) Neuroprotective effects of 7CT, **1**, and **2** against ATP depletion. ATP loss was induced with 20 μM iodoacetic acid (IAA, red). Data are presented as means ± SEM of three independent experiments, and results refer to untreated control cells (black). Statistical analysis was performed using One-way ANOVA followed by Dunnett's multiple comparison post-tests using GraphPad Prism 5 referring to untreated controls in part A or cells treated with the respective insult only in parts B, C, and D (red bars). Levels of significance: * $p < 0.05$; ** $p < 0.01$; *** $p < 0.001$. (E) Effects of 7CT, **1**, and **2** on NO production in LPS-induced neuroinflammation in BV-2 microglial cells. Cells were treated overnight with 50 ng/mL LPS alone or in the presence of 7CT, **1**, or **2**. Supernatants were cleared, and NO was quantified by the Griess assay. Data are given as means ± SEM and relative to BV-2 cells treated with LPS only, which was set as 100%.

challenge due to the minor differences in reactivity of the various hydroxyl groups in flavonoids. It can involve complex sequences of full protection, regioselective deprotection, esterification, and full deprotection. We previously described direct regioselective esterification for both the flavonolignan silibinin and taxifolin.[15,17] Therefore, regioselective esterification with taxifolin was achieved by forming the acid chloride of compound **7** with oxalyl chloride. *In situ* esterification under basic conditions with adjusted reaction times, as described before,[15] and extensive column purification gave the target compound 7CT-alkyne (**1**). 7CT-alkane (**2**) was synthesized as a control to compare the influence of an aliphatic modification in the aromatic position on the neuroprotective performance of the compound and served as a negative control in the CuAAC reaction. The synthetic route for compound **2** was analogous to that of compound **1**, replacing 5-iodopentyne (**3**) with 1-iodopentane in step iii (Scheme 1).

Cell Culture Assays to Confirm a Comparable Mode of Action. To validate the chemical probe, compounds **1** and **2** were subjected to phenotypic screening assays addressing different age-related stresses, as age is the major risk factor of neurodegenerative diseases.[6] Activities of the chemical probe **1** and control compound **2** were investigated in the three different assays oxytosis, ferroptosis, and ATP depletion in the murine hippocampal cell line HT22. Oxytosis is a form of programmed cell death due to oxidative stress induced by intracellular glutathione (GSH) depletion due to glutamate treatment.[24] As GSH reduction is seen in the aging brain and is accelerated in AD, this assay has a mechanistic association with aging and AD.[25] Closely related to oxytosis, if not identical, is the cell death pathway ferroptosis.[26] Here, oxidative stress is induced by direct inhibition of glutathione peroxidase 4 (GPX4) with the compound RSL3. Distinct from oxytosis, which is induced by glutamate inhibiting cysteine import by blocking system x_c^-, ferroptosis is induced downstream in the cascade. ATP depletion is of interest, as the breakdown in neuronal energy production leads to decreased energy metabolism and ATP levels in the aging brain, which is associated with nerve cell damage and death in AD.[27] To induce ATP loss, HT22 cells were treated with iodoacetic acid (IAA), an irreversible inhibitor of the glycolytic enzyme glyceraldehyde 3-phosphate dehydrogenase.

Figure 4 shows the activity of the chemical probe **1** and the control compound **2** compared to that of the lead compound 7-*O*-cinnamoyltaxifolin (7CT). Even though there is a slight increase in toxicity by the introduction of the aliphatic moiety (Figure 4A), compound **1** proved to be neuroprotective throughout all assays, as was control compound **2**. At a concentration of 5 μM, compound **1** was as protective as 7CT in the phenotypic screening assays for protection against oxytosis (Figure 4B), ferroptosis (Figure 4C), and ATP depletion (Figure 4D) proving that the compound is active and therefore suitable for use as a chemical probe for target identification.

https://dx.doi.org/10.1021/acschemneuro.0c00589
ACS Chem. Neurosci. XXXX, XXX, XXX−XXX

Furthermore, we were also interested in whether compound **1** could be effective against neuroinflammation. As shown in Figure 4E, bacterial lipopolysaccharide (LPS)-induced inflammation in BV-2 mouse microglial cells was reduced by compounds **1** and **2**. The production of nitric oxide (NO) as a proinflammatory mediator was quantified to assess inflammation. At 10 μM, the highest concentration tested, NO levels are reduced to around 45% compared to those of LPS treatment alone, confirming the anti-neuroinflammatory effect of **1** and **2**.

The results of the phenotypic screening assays and microglial activation showed that compound **1** was protective in all assays tested and was not altered in its activity compared to that of 7CT, which was of utmost importance for using **1** as a chemical probe. Compound **1** exhibited neuroprotection addressing different characteristics of neurodegeneration and aging in oxytosis, ferroptosis, ATP depletion, and neuroinflammation at low micromolar concentrations.

Intracellular Pathways Are Modified by Compound 1. The nuclear factor (erythroid-derived 2)-like 2 (Nrf2) is an important transcription factor regulating many antioxidant and detoxification enzyme genes. It is the main regulator of the antioxidant response element (ARE) and is crucial for maintaining the cellular redox balance by preventing the accumulation of reactive oxygen species (ROS) and oxidative stress, one of the hallmarks of AD.[28] It has been shown that a taxifolin ester with gallic acid upregulated Nrf2 pathway in RAW264.7 cells,[16] and we previously found 7CT to induce Nrf2 activation in microglial BV-2 cells.[17] Therefore, we asked whether compound **1** also modifies Nrf2 levels. Nuclear fractions of HT22 cells treated with compound **1** and 7CT for comparison were submitted to Western blot analysis. Figure 5 shows that compound **1** significantly induced Nrf2 upregulation. Even though 7CT seemed more potent at higher concentrations and led to nearly a 6-fold induction of Nrf2 levels at 10 μM, increased Nrf2 levels were significant for both compounds at the same concentration of 5 μM (Figure 5B).

Upregulation of Nrf2 is, therefore, one potential mechanism explaining the neuroprotective activity of the compounds. The classical mechanism for Nrf2 activation is by its interaction with Keap1. When bound to Keap1, Nrf2 is directed for proteasomal degradation. Modification on cysteine residues of Keap1, by oxidative stress, for example, leads to dissociation of the complex and translocation of Nrf2 to the nucleus where it activates several cellular responses including the ARE. However, phosphorylation of Nrf2 by various protein kinases can be an alternative mechanism of Nrf2 regulation.[29] It is known that extracellular signal-regulated protein kinase (ERK) can play a role in Nrf2 activation, and levels of ERK phosphorylation are modified by natural products.[30] Furthermore, ERK signaling is involved in cell proliferation, differentiation, and survival or promotion of cell death and therefore can be involved in neurodegeneration.[31] We were interested in whether ERK is activated by compound **1** and 7CT in HT22 cells, as modifications of mitogen-activated protein (MAP) kinases have not been investigated for 7-*O*-esters of taxifolin before. Figure 6 shows a time-course of HT22 cells incubated with 10 μM **1** or 7CT. Both compounds lead to a significant increase in ERK phosphorylation and thereby activation after 5 min (Figure 6B). The effect ceased with increased incubation times thereby excluding chronic ERK activation, which is correlated with neurodegeneration.[32] Another MAP kinase important in the context of AD is p38.

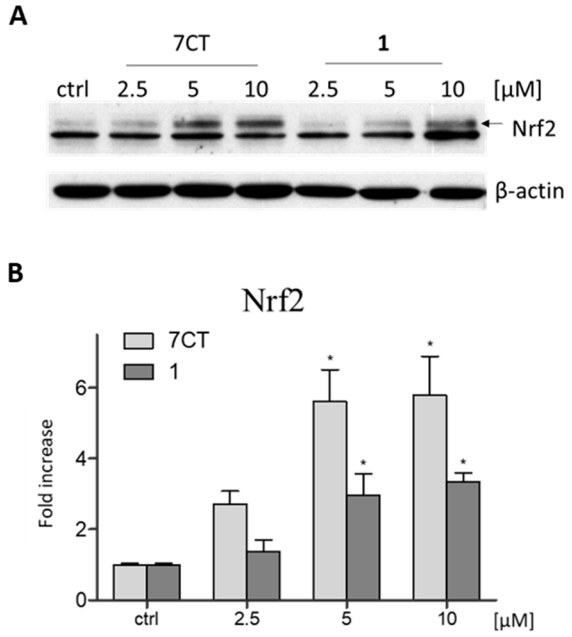

Figure 5. Western blot analysis of Nrf2. Nrf2 induction by 7CT and **1** in nuclear fractions of HT22 cells. (A) Cells were treated for 4 h with DMSO as control or with increasing concentrations of **1** or 7CT. Nuclear fractions of HT22 cells were prepared and analyzed by Western blot for Nrf2. Levels of Nrf2 were normalized to actin, and representative blots are shown. (B) Quantification of the results from three independent experiments as shown in part A. Statistical significance refers to DMSO-treated controls with * $p < 0.05$.

Postmortem brains of early stage AD patients showed increased phosphorylation of p38 which is connected to mediating Aβ-induced inflammation and impaired autophagy in neurons leading to neurodegeneration.[33−35] At a concentration of 10 μM, compound **1** and 7CT both reduce p38 phosphorylation (Figure 6C). Decreased activation was observed after 5 min of incubation and was significantly reduced for the whole time-course of 2 h. The results for activation of ERK and deactivation of p38 underline that 7CT and compound **1** modify MAP kinases. Thus, these results strengthen the reliability of compound **1** as suitable bait for target identification.

CuAAC with Cy3-Azide. The introduction of the alkyne tag in compound **1** enables the reaction of the compound with different azide carriers. As a proof of concept for the CuAAC reaction, and to visualize cellular uptake and the intracellular localization of compound **1**, we coupled **1** to an azide conjugated fluorophore Cy3. First, adducts of the chemical probe **1** with proteins of HT22 lysates were visualized by Western blot analysis. Cy3-azide was coupled to compound **1** in a CuAAC reaction, and bands were detected with an anti-Cy3 antibody. HT22 cells were incubated with increasing concentrations of 5−80 μM **1** for 4 h, lysed, and submitted to the CuAAC reaction using 20 μM Cy3-azide. Incubation of HT22 cells with **1** led to the conjugation of a wide range of proteins with increasing intensity which correlated with increasing concentrations of the compound (see Supporting Information (SI), Figure S1). In cells incubated with DMSO, no adducts were detected. This was also the case for incubation with compound **2** lacking the alkyne tag (SI, Figure S2). Therefore, Cy3-coupling and the detection of conjugated intracellular proteins bound to the probe **1** was

https://dx.doi.org/10.1021/acschemneuro.0c00589
ACS Chem. Neurosci. XXXX, XXX, XXX−XXX

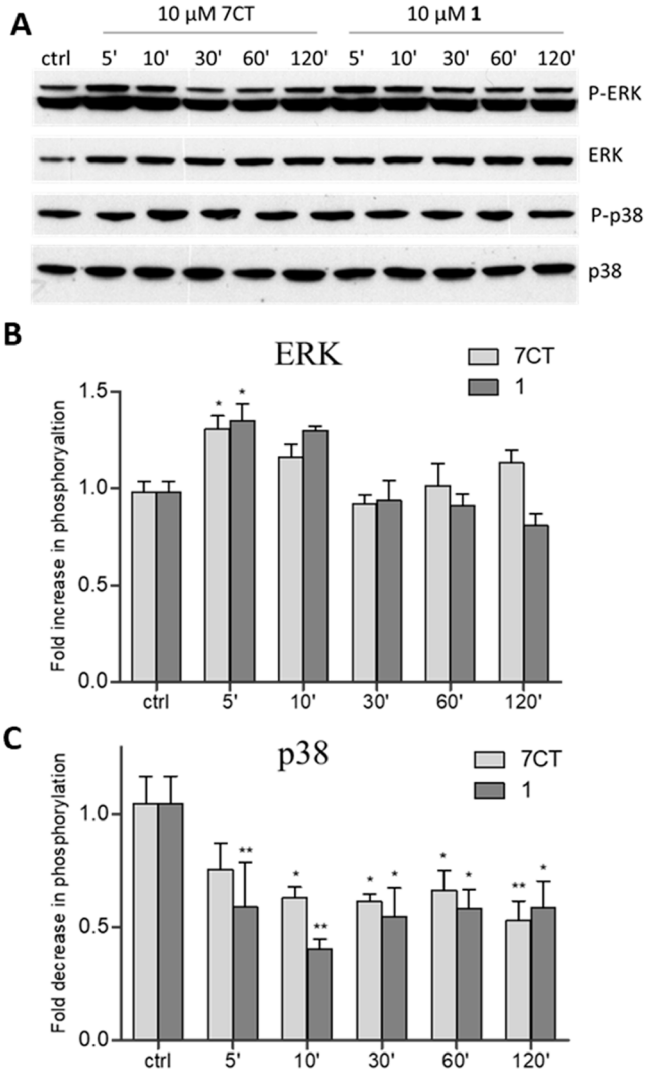

Figure 6. Time-dependent modification of MAP kinases by 7CT and **1** in HT22 cells. (A) Cells were treated for the indicated time points with 10 μM **1** or 7CT. DMSO treatment served as a control. Lysates of HT22 cells were prepared in sample buffer and analyzed by Western blot for phosphorylated ERK (P-ERK), total ERK (ERK), phosphorylated p38 (P-p38), or total p38 (p38). Levels of the phosphorylated protein were normalized to those of the total protein, and representative blots are shown. (B) Quantification of the results from three independent experiments, as shown in part A. Statistical significance refers to DMSO-treated controls with * $p < 0.05$, ** $p < 0.01$.

dependent on the presence of the alkyne moiety and not due to unspecific binding.

Microscopic Analysis. Mitochondria play a crucial role in apoptosis,[36] and in AD, neuronal cell death is associated with mitochondrial dysfunction.[37] Although the exact role of mitochondria in ferroptosis is under debate, increasing evidence strongly suggests that these organelles can also play a key role in this cell death pathway.[38−41] To determine whether compound **1** is targeting the mitochondria, we used fluorescence microscopy to analyze its intracellular location. Therefore, HT22 cells stably expressing the green fluorescent protein in mitochondria (mito-GFP) were incubated with 5 μM compound **1** or DMSO for 30 min, and after fixation, the cells were reacted with Cy3-azide in a CuAAC reaction. The specimens were then imaged by high-resolution fluorescence microscopy using an Airyscan detector.[42] As shown in Figure 7, compound **1** is found at several locations after 30 min of incubation, including in unknown structures in the perinuclear region. Importantly, the fluorescence profiles of mito-GFP and Cy3 indicate that compound **1** is also strongly enriched in mitochondria after 30 min of incubation (see graphs on the right of Figure 7). No significant signal for Cy3 was detected in control cells treated with DMSO. These results indicate that the interaction partners of compound **1** and 7CT might be associated with mitochondria.

Affinity Pulldown and MS Analysis. After demonstrating that compound **1** is suitable as a chemical probe for 7CT, due to pronounced neuroprotection by the same mode of action, the chemical probe **1** was applied for target identification in an affinity pulldown with HT22 cells. HT22 cells were incubated with 200 μM of compound **1** or DMSO as a control for 2 h before lysis and the CuAAC reaction with biotin-azide. Proteins bound by **1** and the DMSO-control lysates were purified on streptavidin magnetic beads, separated by SDS−PAGE, and analyzed by nanoLC−MS/MS after tryptic digestion in a label-free quantification. A total of 708 proteins were identified and quantified. Of these, 70 were significantly enriched in both replicates and thus classified as potential target candidates (summed significance 4; Figure 8). Two of the 70 hits were pursued further to investigate the interaction between compound **1** and 7CT and the respective identified proteins. One was the sarco/endoplasmic reticulum Ca^{2+}-ATPase (SERCA, Atp2a2), which was the protein with the highest significance in the log2 protein ratio sample/control and therefore the top target identified according to MS analysis (Figure 8). As the microscopic analysis showed localization of compound **1** in mitochondria, we were interested in mitochondrial proteins among the targets. Indeed, the mitochondrial carrier adenine nucleotide translocase 1 (ANT-1, Slc25a4) was among the top 4 most significant hits and was chosen as a second target for further examination.

ANT-1 and SERCA Are Identified in MS Analysis. Adenine nucleotide translocase-1 (ANT-1) was identified as a potential target in MS/MS analysis. This finding is supported by the microscopic analysis conducted, where colocalization of Cy3-labeled **1** with mitochondria was observed (Figure 7). ANT-1 is an ADP/ATP carrier at the inner mitochondrial membrane and the most abundant protein in mitochondria, contributing to 1−10% of total mitochondrial protein.[43] ANT-1 is the muscle and brain-specific isoform of ANT and is important for mitochondrial physiology as well as general cell function, as it transports ADP into the mitochondrial matrix and ATP into the cytoplasm, undergoing extensive conformational changes during transport.[44−46] ANT-1 is relevant as a potential pharmacological target in the context of neurodegenerative disorders, particularly for AD, as mitochondrial dysfunction is proposed to be one of the major hallmarks of the disease.[47,48] ANT-1 has been studied in the context of apoptosis as well. The carrier was characterized as a proapoptotic protein, as increased ATP export, which is important for apoptosis, is mediated by enhanced levels of ANT-1 leading to mitochondrial breakdown and the apoptotic cascade.[45,49,50] Its role in nonapoptotic forms of cell death, like ferroptosis and oxytosis covered in this work, has not been described so far. Therefore, HT22 cells transfected with ANT-1 siRNA were tested for effects on oxytosis and ferroptosis. ANT-1 knockdown protected against these insults. Significantly more cells survived treatment with glutamate as an

https://dx.doi.org/10.1021/acschemneuro.0c00589
ACS Chem. Neurosci. XXXX, XXX, XXX−XXX

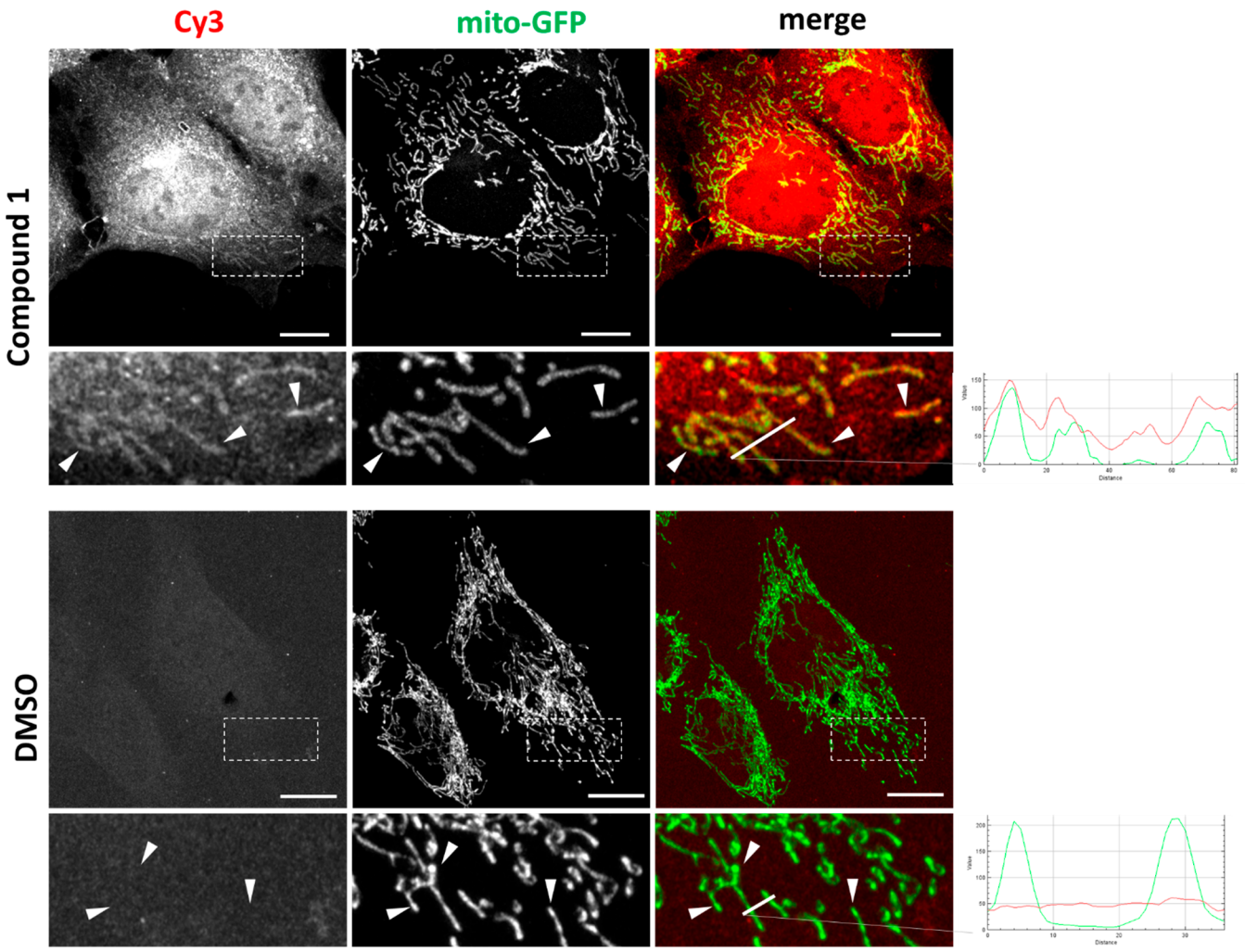

Figure 7. Microscopic analysis of HT22-mitoGFP cells with compound **1**. Representative microscopic images of HT22-mitoGFP cells incubated with 5 μM **1** or DMSO for 30 min. Red signals derive from Cy3 and correspond to adducted proteins; green signals are mitochondria-targeted GFP. Arrows indicate mitochondrial structures to note the colocalization of Cy3 staining with mitochondria in cells incubated with compound **1** compared to the absence of a signal in DMSO-treated cells. To visualize the colocalization, a line was plotted in the merged images (magnified images). Charts on the right show quantification of the fluorescence profile along this line for each channel. The *X*-axis indicates distance, and the *Y*-axis represents fluorescence intensity in arbitrary units. Bars = 10 μm.

inducer of oxytosis (Figure 9A), or erastin and RSL3 as inducers of ferroptosis (Figure 9B,C, respectively). These findings strongly support the implication of ANT-1 inhibition in the protective effect of compound **1** and consequently 7CT.

The treatment of ANT-1 knockdown cells with 7CT in oxytosis conditions induced by glutamate showed that the compound provides additional protection (Figure 9E). In the absence of 7CT, the knockdown of ANT-1 is significantly protective. However, upon treatment of 7CT, the control cells are as protected as the ANT-1 knockdown cells indicating that ANT-1 is not the exclusive target of 7CT, and other mechanisms are also involved in the protection (Figure 9E). ROS and oxidative stress lead to increased mitochondrial membrane potential (MMP).[51] It was shown that FCCP, a mitochondrial uncoupler dissipating the MMP, also protects cells from oxytosis.[52] Furthermore, a study with quercetin showed that low concentrations of the flavonoid reduced the MMP and inhibited adenine nucleotide exchange by ANT-1.[53] As the concentrations at which neuroprotection is observed in our study are in the low micromolar range, we hypothesize that **1** and 7CT could act as mild uncouplers and inhibitors of ANT-1 and thereby protect cells. It has been reported that the nucleotide exchange by ANT-1 can potentially play a role in maintaining the MMP,[54,55] but increased oxidative damage by apoptosis inducers leads to harmfully increased expression levels of ANT-1.[56,57] However, whether this is also the case for oxytosis and ferroptosis as well as the exact role of ANT-1 in these nonapoptotic pathways remains a subject of future research.

A second interaction partner identified by MS analysis was the sarco/endoplasmic reticulum Ca^{2+}-ATPase 2 (SERCA). Located in the endoplasmic reticulum (ER), the pump regulates calcium influx into the ER under ATP consumption. ER-stress concomitant with calcium dysregulation causes neuronal impairment and death and is involved in the progressive neurological decline of AD.[58] Krajnak et al. showed that activation of SERCA is neuroprotective and improves memory and cognition in APP/PS1 mice.[59] In this work, SERCA was validated as a target for 7-*O*-esters of taxifolin by knockdown experiments. In contrast to the results with ANT-1, HT22 cells treated with SERCA siRNA were not protected against glutamate-induced oxytosis (Figure 9D). However,

https://dx.doi.org/10.1021/acschemneuro.0c00589
ACS Chem. Neurosci. XXXX, XXX, XXX−XXX

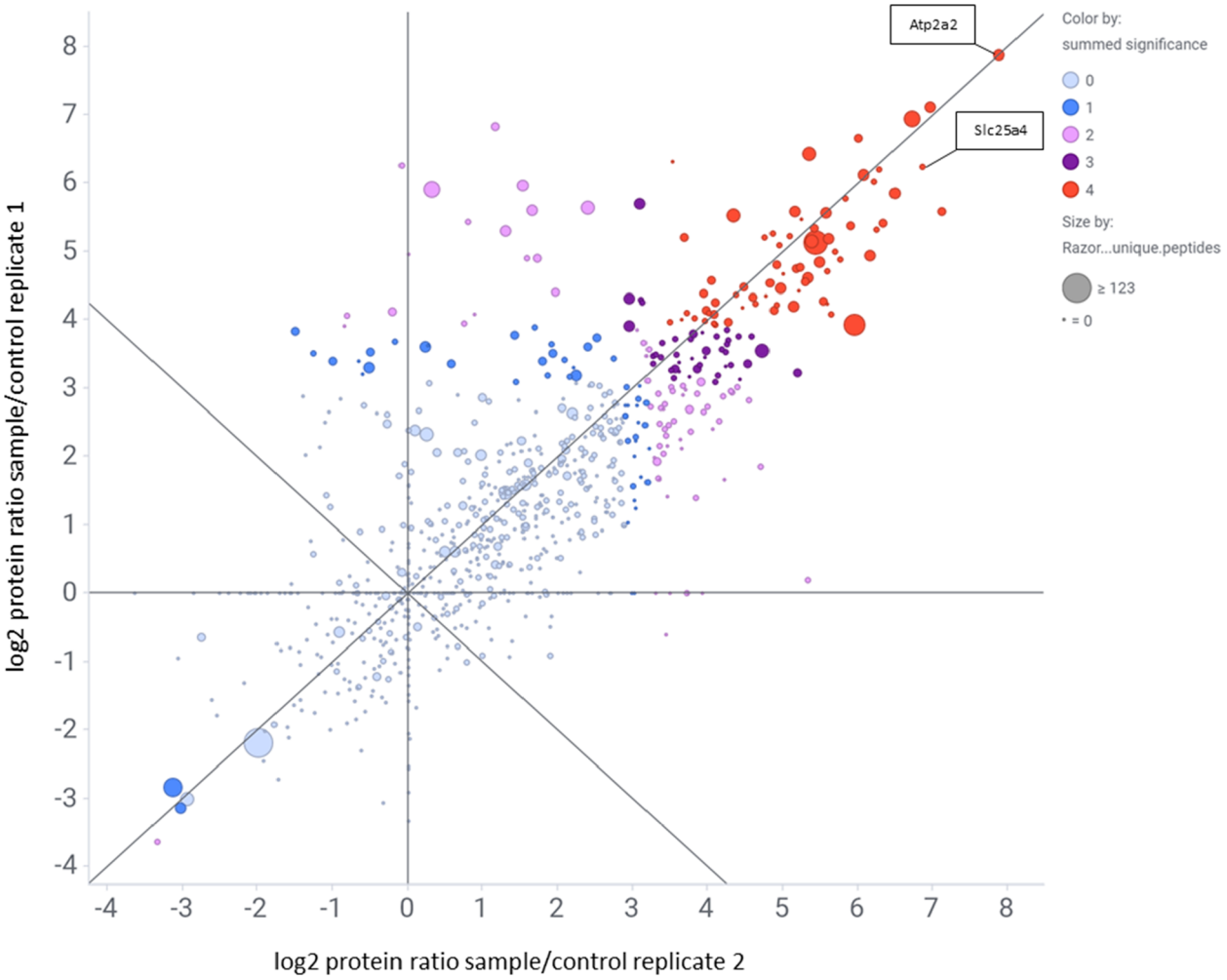

Figure 8. Mass spectrometric identification of target candidates. Log2 transformed protein ratios sample/control of two replicates are shown. Summed significance values were used to identify the best target candidates (significance 2 in both replicates = significance 4, marked in red). The size of the dots corresponds to the number of razors and unique peptides of a protein.

SERCA knockdown significantly impaired the protection by compound 7CT at the lower concentrations of 2.5 and 5 μM (Figure 9E) suggesting an important role of SERCA in the protective mechanism of 7CT. At a concentration of 10 μM 7CT, the decrease in protection by the absence of SERCA was no longer seen. Higher concentrations of 7CT likely activate other protective pathways due to the pleiotropic action of the compound and hence compensate for SERCA knockdown.

CONCLUSION

In summary, a chemical probe of the neuroprotective natural product hybrid 7-*O*-cinnamoyltaxifolin bearing an alkyne tag for CuAAC reaction was designed and synthesized. The probe **1** proved its suitability as a neuroprotectant in cell-based phenotypic screening assays addressing different aspects of neurodegeneration and aging. On a molecular level, Western blots were used to confirm that the parent compound and the probe act on the same pathways and to ensure that the alkyne tag was not altering the mechanisms of action. Both compounds, **1** and 7CT, induced significant upregulation of Nrf2 in HT22 nuclear fractions, increased ERK phosphorylation, and reduced phosphorylation of p38 in HT22 lysates. Microscopic analysis of **1** coupled to the fluorescent dye Cy3-azide showed efficient uptake of the compound into HT22 cells and localization in mitochondria. MS analysis after CuAAC of **1** with biotin-azide and following streptavidin purification, revealed 70 potential target candidates by MS analysis. Due to the pleiotropic mechanism of action, the identification of many interaction partners was assumed. As compound **1** carries a Michael system, which is prone to react with nucleophiles like thiols, we expected to identify proteins that were previously described to interact with electrophiles.[21] HSP90, prohibitin, and 14-3-3β are examples of such proteins. Indeed, HSP90, prohibitin and 14-3-3β were identified among others in the MS analysis of the pulldown with compound **1** (for the full list of targets, see Supporting Information). However, the top target candidate of compound **1** in MS analysis was SERCA. In addition, because microscopic analysis pointed at mitochondria as a subcellular location for compound **1**, we also looked at the top mitochondrial target candidate in the analysis which was the mitochondrial protein ANT-1. These two proteins were chosen to investigate for their relevance as targets of compound **1** and 7CT in knockdown experiments. As both proteins are crucial for cell homeostasis and survival and are for the first time shown to be modified by 7-*O*-esters of flavonoids, further work in this area should focus on the role of ANT-1 and SERCA in AD and oxytotic/ferroptotic cell death pathways as well as the

https://dx.doi.org/10.1021/acschemneuro.0c00589
ACS Chem. Neurosci. XXXX, XXX, XXX−XXX

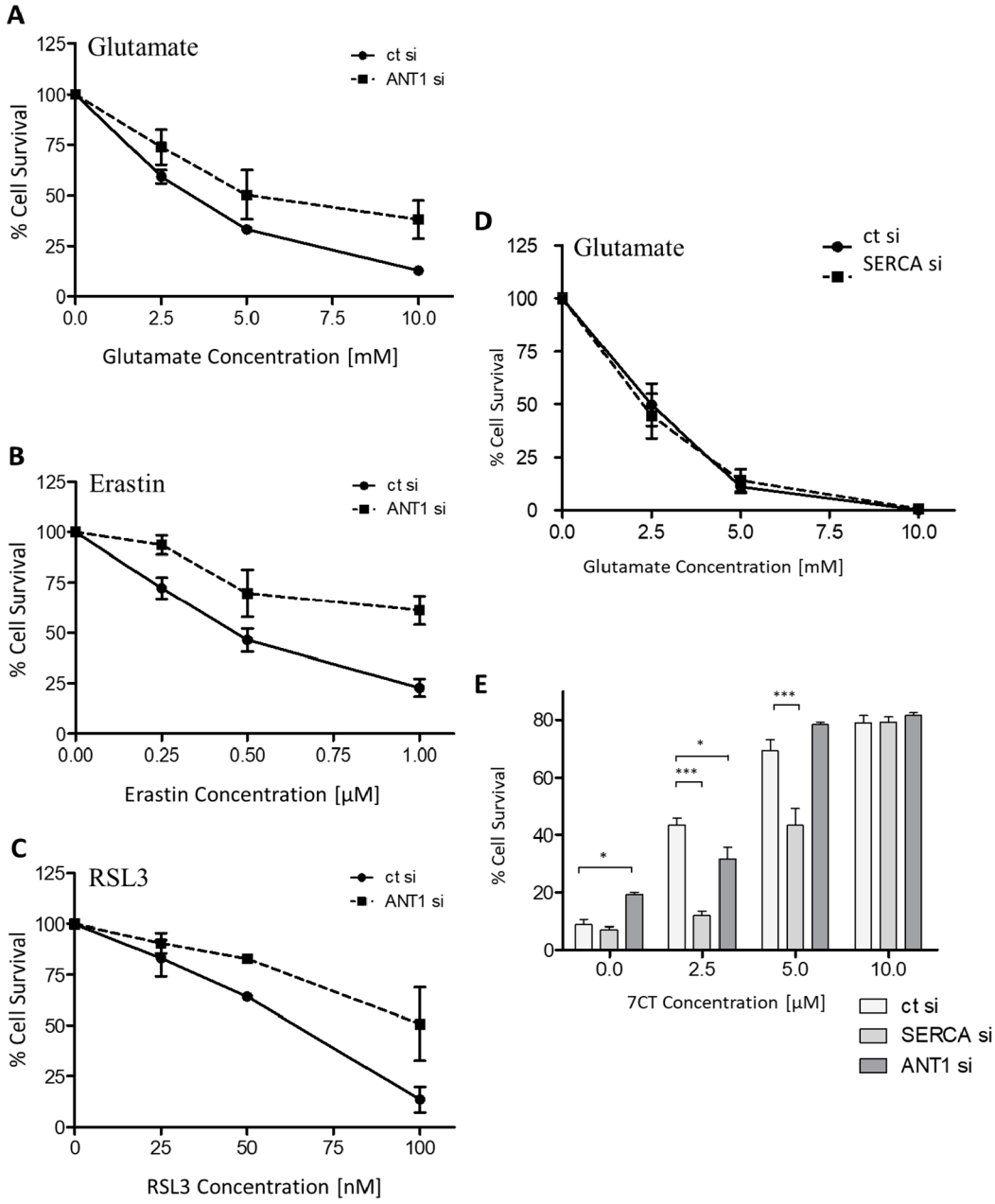

Figure 9. Transfection of HT22 cells with ANT-1 siRNA and SERCA siRNA and investigations on neuroprotection. ANT-1 knockdown leads to protection against glutamate as an inducer of oxytosis (A), and erastin (B) and RSL3 (C) as inducers of ferroptosis. (D) The transfection of HT22 cells with SERCA siRNA is not protective against glutamate-induced oxytosis. (E) ANT-1 (dark gray) and SERCA (light gray) knockdown cells were treated with increasing concentrations of 7CT in the presence of glutamate. Data are presented as means ± SEM of four independent experiments. Statistical analysis was rendered using Two-way ANOVA followed by Bonferroni posttests using GraphPad Prism 5. Levels of significance: * $p < 0.05$; *** $p < 0.001$.

identification and functional characterization of the site(s) modified by the compound. Our findings are a step toward understanding the specific interaction partners of natural product-derived compounds like 7-*O*-esters of flavonoids. The activity-based protein profiling approach with compound **1** as a chemical probe revealed several proteins as interaction partners that might also apply to other flavonoids and lead to new approaches for drug development against neurodegenerative diseases like AD.

METHODS

Chemical Synthesis. *General Information.* All reagents were used without further purification and bought from common commercial suppliers in reagent grade. For anhydrous reaction conditions, THF was dried before use by refluxing over sodium slices for at least 2 days under an argon atmosphere. Thin-layer chromatography was performed on silica gel 60 (alumina foils with fluorescent indicator 254 nm). UV light (254 and 366 nm) was used for detection. For column chromatography, silica gel 60 (particle size 0.040−0.063 mm) was used. Nuclear magnetic resonance (NMR) spectra were recorded with a Bruker AV-400 NMR instrument (Bruker, Karlsruhe, Germany) in a deuterated solvent. Chemical shifts are expressed in parts per million (ppm) relative to the solvent applied (2.50 ppm for 1H and 39.5 ppm for 13C in DMSO-d_6; 7.26 ppm for 1H and 77.2 ppm for 13C for $CDCl_3$; 2.05 ppm for 1H and 206.3 ppm for 13C for acetone-d_6; 4.87 ppm for 1H and 49.0 ppm for 13C for methanol-d_4). The purity of the synthesis products was

https://dx.doi.org/10.1021/acschemneuro.0c00589
ACS Chem. Neurosci. XXXX, XXX, XXX−XXX

determined by HPLC (Shimadzu Products), containing a DGU-20A3R degassing unit, an LC20AB liquid chromatograph, and an SPD-20A UV/vis detector. UV detection was measured at 254 nm. Mass spectra were obtained by an LCMS 2020 (Shimadzu Products). As a stationary phase, a Synergi 4U fusion-RP (150 mm × 4.6 mm) column was used, and as a mobile phase, a gradient of methanol/water with 0.1% formic acid was used. Parameters: A = water, B = methanol, $V(B)/(V(A) + V(B))$ = from 5 to 90% over 10 min, $V(B)/(V(A) + V(B))$ = 90% for 5 min, $V(B)/(V(A) + V(B))$ = from 90 to 5% over 3 min. The method was performed with a flow rate of 1.0 mL/min. Compounds were only used for biological evaluation if the purity was ≥95%. Melting points were determined using an OptiMelt automated melting point system (Scientific Instruments GmbH, Gilching, Germany).

General Procedure A: Protection. Acid (1.0 equiv) was dissolved in ethanol, and H_2SO_4 was added. The solution was refluxed until TLC showed full conversion. The reaction mixture was concentrated *in vacuo* and dissolved in ethyl acetate to be washed with 5% sodium hydrogen carbonate in water. The organic layers were combined, and the solvent was evaporated.

General Procedure B: Substitution. K_2CO_3 (1.5 equiv) was dissolved in dry acetone under argon and cooled to 0 °C in an ice bath when the protected acid (1.0 equiv) was added. The mixture was stirred at 0 °C for 15 min, and the respective iodine (2.0 equiv) was added. The reaction was heated to reflux for 6 h, diluted with water and 1 M HCl, extracted with ethyl acetate (3 × 30 mL), washed with brine, and dried over Na_2SO_4. The solvent was removed, and the compound was purified by silica column chromatography using 20% ethyl acetate in petroleum ether to give the compound as an oil.

General Procedure C: Deprotection. The compound was dissolved in ethanol, and 0.52 M NaOH was added. The mixture was stirred at room temperature for 5 h. The reaction was diluted with 5 mL of water and extracted with ethyl acetate twice. The aqueous layers were combined and acidified to pH 1 with 1 M HCl to be again extracted with ethyl acetate. The organic layers were combined, washed with brine, and dried over Na_2SO_4.

General Procedure D: Esterification. Acid (1.1 equiv) was dissolved in 5 mL of dry THF, and oxalyl chloride (2.0 equiv) together with catalytic amounts of DMF (4 μL) were added. The reaction was stirred at room temperature until TLC showed complete conversion of the acid to the acid chloride. The acid chloride was then added dropwise to a solution of taxifolin (1.0 equiv) and triethylamine (4.5 equiv) in dry THF and stirred at room temperature for 2 h. The reaction was quenched with water and 1 M HCl and extracted with ethyl acetate. The organic layer was combined, washed with brine, and dried over Na_2SO_4. The mixture was purified by flash column chromatography using a gradient of 4−15% acetone in dichloromethane to give the pure compound.[15,17]

*5-Iodo Pentyne (**3**).* 5-Chloro pentyne (1.0 g, 9.76 mmol, 1.0 equiv) was dissolved in dry acetone, and sodium iodine (7.3 g, 48.8 mmol, 5.0 equiv) was added; the mixture was heated to reflux overnight. The reaction was diluted with water and extracted with dichloromethane (3 × 40 mL). The organic layer was combined, washed with brine, and dried over Na_2SO_4, and the solvent was evaporated. The compound was obtained as a yellow oil (1.8 g, quantitative (quant)).

^{1}H NMR (400 MHz, $CDCl_3$): δ 3.28 (td, *J* = 6.7, 1.3 Hz, 2H), 2.34−2.26 (m, 2H), 2.01−1.92 (m, 3H) ppm.

^{13}C NMR (101 MHz, $CDCl_3$): δ 82.4 (s), 69.6 (s), 32.0 (s), 19.6 (s), 5.2 (s) ppm.

*Ethyl (E)-3-(3-Hydroxyphenyl)acrylate (**5**).* Following general procedure A, 500 mg of *trans*-3-hydroxycinnamic acid was dissolved in 15 mL of ethanol, and 5 drops of sulfuric acid were added. After 6 h, TLC showed total consumption of the educt. Compound **5** was obtained as an off-white solid (584 mg, quant).

^{1}H NMR (400 MHz, acetone-d6): δ 8.54 (s, 1H, −OH), 7.60 (d, *J* = 16.0 Hz, 1H, *H*C═CHCO), 7.26 (t, 1H, aromatic (arom)), 7.15−7.11 (m, 2H, arom), 6.93−6.90 (m, 1H, arom), 6.43 (d, *J* = 16.0 Hz, 1H, HC═C*H*CO), 4.20 (quart, 2H, OCH_2CH$_3$), 1.28 (t, 3H, OCH$_2$CH_3) ppm.

^{13}C NMR (101 MHz, acetone-d6): δ 167.0, 158.7, 145.2, 136.8, 130.9, 120.5, 119.10, 118.3, 115.4, 60.8, 14.6 ppm.

*Ethyl (E)-3-(3-(Pent-4-yn-1-yloxy)phenyl)acrylate (**6**).* Following general procedure B, **5** (300 mg, 1.5 mmol, 1.0 equiv) was reacted with **3** (605 mg, 3.12 mmol, 2.0 equiv) and K_2CO_3(311 mg, 2.25 mmol, 1.5 equiv). Compound **6** was obtained as a yellow oil (352 mg, 1.36 mmol, 91% yield).

^{1}H NMR (400 MHz, $CDCl_3$): δ 7.64 (d, *J* = 16.0 Hz, 1H, *H*C═CHCO), 7.27 (t, 1H, arom), 7.11 (m, 1H, arom), 7.05 (m, 1H, arom), 6.93−6.91 (m, 1H, arom), 6.41 (d, *J* = 16.0 Hz, 1H, HC═C*H*CO), 4.26 (quart, 2H, OCH_2CH$_3$), 4.08 (t, 2H, H≡CCH$_2$CH$_2$CH_2O), 2.40 (dt, 2H, H≡CCH$_2$CH_2CH$_2$O), 2.03−1.97 (m, 3H, *H*≡CCH_2CH$_2$CH$_2$O), 1.33 (t, 3H, OCH$_2$CH_3) ppm.

^{13}C NMR (101 MHz, $CDCl_3$): δ 167.0, 159.3, 144.6, 135.9, 130.0, 120.9, 118.7, 116.8, 113.6, 83.4, 69.1, 66.3, 60.6, 28.2, 15.2, 14.4 ppm.

*(E)-3-(3-(Pent-4-yn-1-yloxy)phenyl)acrylic Acid (**7**).* Following general procedure C, 290 mg **6** was dissolved in 3 mL of ethanol, and 5 mL of 0.52 M NaOH was added. The compound was obtained as a white solid (191 mg, 0.82 mmol, 73% yield).

^{1}H NMR (400 MHz, $CDCl_3$): δ 7.74 (d, *J* = 16.0 Hz, 1H, *H*C═CHCO), 7.31 (t, 1H, arom), 7.15 (d, *J* = 8.0 Hz 1H, arom), 7.08 (m, 1H, arom), 6.97 (dd, *J* = 8.0 and 2.3 Hz, 1H, arom), 6.46 (d, *J* = 16.0 Hz, 1H, HC═C*H*CO), 4.11 (t, 2H, H≡CCH$_2$CH$_2$CH_2O), 2.42 (td, 2H, H≡CCH$_2$CH_2CH$_2$O), 2.06−1.98 (m, 3H, *H*≡CCH_2CH$_2$CH$_2$O) ppm.

^{13}C NMR (101 MHz, $CDCl_3$): δ 172.0, 159.3, 147.0, 135.4, 130.0, 121.2, 117.5, 117.2, 113.8, 83.3, 69.0, 66.3, 28.1, 15.2 ppm.

*7-O-Cinnamoyltaxifolin-pentyne (**1**).* Following general procedure D, **7** (120 mg, 0.52 mmol, 1.1 equiv) was dissolved in 5 mL of dry THF, and 85 μL of oxalyl chloride (127 mg, 1.00 mmol, 2 equiv) and catalytic amounts of DMF were added. Taxifolin (150 mg, 0.52 mmol, 1 equiv) and triethylamine (228 mg, 2.25 mmol, 4.5 equiv) were dissolved in dry THF, and the acid chloride was added dropwise. Target compound **1** was obtained as a white foam (137 mg, 0.26 mmol, 53% yield).

^{1}H NMR (400 MHz, DMSO-d6): δ 11.73 (s, 1H, 5-OH), 9.03 (s, 2H, 3′ and 4′-OH), 7.80 (d, *J* = 16.0 Hz, 1H, ArC*H*═CH−CO), 7.40 (s, 1H, arom CA), 7.35 (d, *J* = 5.1 Hz, 2H, arom CA), 7.05−7.02 (m, 1H, arom CA), 6.93 (m, 1H, arom B-ring), 6.88 (d, *J* = 16.0 Hz, 1H, ArCH═C*H*−CO), 6.79−6.76 (m, 2H, arom B-ring), 6.45 (d, *J* = 2.0 Hz, 1H, 8-H), 6.42 (d, *J* = 2.0 Hz, 1H, 6-H), 5.92 (d, *J* = 6.2 Hz, 1H, 3-OH), 5.15 (d, *J* = 11.6 Hz, 1H, 2-H), 4.70 (dd, *J* = 11.5, 6.3 Hz, 1H, 3-H), 4.09 (t, 2H, HC≡C−CH$_2$−CH$_2$−CH_2), 2.80 (t, 1H, *H*C≡C−CH$_2$−CH$_2$−CH$_2$), 2.34 (td, *J* = 2.6 Hz, 2H, HC≡C−CH_2−CH$_2$−CH$_2$), 1.90 (tt, *J* = *J*′ = 6.5 Hz, 2H, HC≡C−CH$_2$−CH_2−CH$_2$) ppm.

^{13}C NMR (101 MHz, DMSO-d6): δ 199.6, 164.0, 162.0, 161.9, 158.9, 158.1, 147.2, 146.0, 145.0, 135.2, 130.1, 127.7, 121.5, 119.6, 117.7, 117.1, 115.5, 115.2, 113.8, 104.9, 102.8, 101.7, 83.7, 83.3, 71.9, 71.6, 66.2, 27.7, 14.5 ppm.

ESI: *m*/*z* calculated for $C_{29}H_{24}O_9$ $[M + H]^+$ 517.14, found 517.13; HPLC purity = 99%.

*Ethyl (E)-3-(3-(Pentyloxy)phenyl)acrylate (**8**).* Following general procedure B, **5** (500 mg, 2.6 mmol, 1.0 equiv) was reacted with 1-iodopentane (1.03 g, 5.2 mmol, 2.0 equiv) and K_2CO_3(539 mg, 3.9 mmol, 1.5 equiv). Compound **8** was obtained as an off-white oil (330 mg, 1.26 mmol, 48% yield).

^{1}H NMR (400 MHz, $CDCl_3$): δ 7.87 (d, *J* = 16.0 Hz, 1H), 7.49 (t, 1H), 7.30 (d, *J* = 7.9 Hz, 1H), 7.13 (dd, *J* = 7.9, 2.4 Hz, 1H), 6.64 (d, *J* = 16.0 Hz, 1H), 4.48 (q, *J* = 7.1 Hz, 2H), 4.18 (t, 2H), 2.01 (quint, 2H), 1.72−1.59 (m, 4H), 1.56 (t, *J* = 7.1 Hz, 3H), 1.21−1.11 (m, 3H) ppm.

^{13}C NMR (101 MHz, $CDCl_3$): δ 167.0, 159.5, 144.6, 135.8, 129.8, 120.6, 118.4, 116.7, 113.5, 68.1, 60.5, 28.9, 28.2, 22.5, 14.3, 14.0 ppm.

*(E)-3-(3-(Pentyloxy)phenyl)acrylic Acid (**9**).* Following general procedure C, 250 mg of **8** was dissolved in 5 mL of ethanol, and 5 mL of 0.52 M NaOH was added. The compound was obtained as a white solid (173 mg, 1.35 mmol, quant).

^{1}H NMR (400 MHz, $CDCl_3$): δ 7.76 (d, *J* = 15.9 Hz, 1H), 7.31 (t, *J* = 7.9 Hz, 1H), 7.13 (d, *J* = 7.7 Hz, 1H), 7.07 (s, 1H), 6.96 (dd, *J* = 8.2, 2.4 Hz, 1H), 6.44 (d, *J* = 15.9 Hz, 1H), 3.98 (t, *J* = 6.6 Hz, 2H),

https://dx.doi.org/10.1021/acschemneuro.0c00589
ACS Chem. Neurosci. XXXX, XXX, XXX−XXX

1.86−1.75 (m, 2H), 1.54−1.33 (m, 4H), 0.95 (t, J = 7.1 Hz, 3H) ppm.

^{13}C NMR (101 MHz, $CDCl_3$): δ 172.3, 159.7, 147.3, 135.5, 130.1, 121.1, 117.5, 117.4, 113.9, 68.3, 29.1, 28.3, 22.6, 14.2 ppm.

*7-O-Cinnamoyltaxifolin-pentane (**2**).* Following general procedure D, **9** (134 mg, 0.57 mmol, 1.1 equiv) was dissolved in 5 mL of dry THF, and 100 μL of oxalyl chloride (155 mg, 1.08 mmol, 2 equiv) and catalytic amounts of DMF were added. Taxifolin (164 mg, 0.54 mmol, 1 equiv) and triethylamine (278 mg, 2.75 mmol, 4.5 equiv) were dissolved in dry THF, and the acid chloride was added dropwise. Compound **2** was obtained as a white foam (181 mg, 0.35 mmol, 64% yield).

^{1}H NMR (400 MHz, DMSO-d6): δ 11.73 (s, 1H, 5-OH), 9.06 (s, 1H, 3′-OH), 9.00 (s, 1H, 4′-OH), 7.82 (d, J = 16.0 Hz, 1H, ArC*H*═CH−CO), 7.38 (s, 1H, arom H CA), 7.34−7.33 (m, 2H, arom H CA), 7.03−7.00 (m, 1H, arom H CA), 6.93 (m, 1H, arom B-ring), 6.88 (d, J = 16.0 Hz, 1H, ArCH = C*H*−CO), 6.79−6.74 (m, 2H, arom B-ring), 6.45 (d, J = 2.0 Hz, 1H, 8-H), 6.41 (d, J = 2.0 Hz, 1H, 6-H), 5.90 (d, J = 6.3 Hz, 1H, 3-OH), 5.13 (d, J = 11.6 Hz, 1H, 2-H), 4.69 (dd, J = 11.6, 6.3 Hz, 1H, 3-H), 4.01 (t, 2H, $CH_3CH_2CH_2CH_2CH_2O$), 1.72 (tt, J = J' = 6.8 Hz, 2H, $CH_3CH_2CH_2CH_2CH_2O$), 1.43−1.30 (m, 4H, $CH_3CH_2CH_2CH_2CH_2O$), 0.89 (t, 3H, $CH_3CH_2CH_2CH_2CH_2O$) ppm.

^{13}C NMR (101 MHz, DMSO-d6): δ 199.6, 164.0, 162.0 161.9, 159.1, 158.1, 147.2, 146.0, 145.0, 135.1, 130.0, 127.7, 121.3, 119.6, 117.7, 117.0, 115.5, 115.2, 113.7, 104.8, 102.8, 101.7, 83.3, 71.9, 67.6, 28.4, 27.7, 21.9, 13.9 ppm.

ESI: m/z calculated for $C_{29}H_{28}O_9$ $[M + H]^+$ 521.17, found 521.14; HPLC purity = 96%.

Cell Culture General Procedures. HT22 cells were grown in Dulbecco's Modified Eagle Medium (DMEM, Sigma-Aldrich, Munich, Germany) supplemented with 10% (v/v) fetal calf serum (FCS) and 1% (v/v) penicillin−streptomycin. BV-2 cells were grown in low-glucose DMEM (Invitrogen, Carlsbad, CA, USA) supplemented with 10% FCS and 1% (v/v) penicillin−streptomycin. Cells were subcultured every 2 days and incubated at 37 °C with 10% CO_2 in a humidified incubator.

Compounds were dissolved in dimethyl sulfoxide (DMSO, Sigma-Aldrich, Munich, Germany) as stock solutions and diluted further into 1x phosphate-buffered saline (PBS).

For determination of cell viability, a colorimetric 3-(4,5-dimethylthiazol-2-yl)-2,5- diphenyl tetrazolium bromide (MTT, Sigma-Aldrich, Munich, Germany) assay was used. MTT solution (5 mg/mL in PBS) was diluted 1:10 with medium and added to the wells after removal of the old medium. Cells were incubated for 3 h, and then lysis buffer (10% SDS) was applied. The next day, absorbance at 560 nm was determined with a multiwell plate photometer (Tecan, SpectraMax 250).

Neurotoxicity and Oxytosis in HT22 Cells. Cells (5×10^3 cells per well) were seeded into sterile 96-well plates and incubated overnight. For the neurotoxicity assay, the medium was removed, and 1, 5, 10, or 25 μM of the compound diluted with medium from a 0.1 M stock solution was added to the wells. DMSO (0.05%) in DMEM served as a control. Cells were incubated for 24 h at which neurotoxicity was determined using the colorimetric MTT assay.

For the oxytosis assay, 3×10^3 cells per well were treated with 5 mM glutamate (monosodium-*L*-glutamate, Sigma-Aldrich, Munich, Germany) together with 1, 5, or 10 μM concentrations of the respective compounds and incubated for 24 h. Cell viability was determined using the MTT assay, as described above. Results are presented as percentage of untreated control cells. Data are expressed as means ± SEM of three independent experiments. The analysis was accomplished using GraphPad Prism 5 Software applying One-way ANOVA followed by Dunnett's multiple comparison posttest. Levels of significance: * $p < 0.05$; ** $p < 0.01$; *** $p < 0.001$.

Ferroptosis in HT22 Cells. Cells (3×10^3 cells per well) were seeded into sterile 96-well plates and incubated overnight. The next day, the medium was exchanged with fresh medium, and 300 nM RSL3 was added with vehicle (DMSO) to induce oxidative stress, or together with 1, 5, or 10 μM concentrations of the respective compound for protection. After 24 h, cell viability was determined using the MTT assay. Results are presented as percentages of untreated control cells. Data are expressed as means ± SEM of three independent experiments. The analysis was accomplished using GraphPad Prism 5 Software applying One-way ANOVA followed by Dunnett's multiple comparison posttest. Levels of significance: * $p < 0.05$; ** $p < 0.01$; *** $p < 0.001$.

ATP Depletion in HT22 Cells. Cells (3×10^3 cells per well) were seeded into sterile 96-well plates and incubated overnight. The next day, medium was exchanged with fresh medium. Iodoacetic acid (IAA, 20 μM) was added with vehicle (DMSO) as a negative control, or together with 1, 5, or 10 μM concentrations of the respective compound for protection. After 2 h of incubation at 37 °C in the incubator, the medium was aspirated, and fresh medium was applied; only the compounds at the same respective concentrations were added without IAA. After 24 h, cell viability was determined using the MTT assay. Results are presented as percentages of untreated control cells. Data are expressed as means ± SEM of three independent experiments. The analysis was accomplished using GraphPad Prism 5 Software applying One-way ANOVA followed by Dunnett's multiple comparison posttest. Levels of significance: * $p < 0.05$; ** $p < 0.01$; *** $p < 0.001$.

Anti-Inflammatory Activity in BV-2 Cells. Cells (5×10^5 cells per plate) were seeded in sterile 35 mm cell culture dishes. After overnight incubation, medium was exchanged with fresh medium. The cells were pretreated with the respective compounds at the indicated concentrations for 30 min when 50 μg/mL bacterial lipopolysaccharide (LPS) was added. After 24 h of incubation, the medium was collected and spun briefly to remove floating cells, and 100 μL of the supernatant was assayed for nitrite using 100 μL of the Griess Reagent in a 96-well plate. After incubation for 10 min at room temperature, the absorbance at 550 nm was read on a microplate reader. Results are normalized to cell number as assessed by the MTT assay, as described above.

Western Blots. *Sample Preparation.* Cells (1.5×10^5HT22 cells per 35 mm dish) were grown for 24 h before treatment with the respective compounds at the indicated concentrations and incubation times. For whole lysate analysis, cells were washed twice with PBS and scraped into 100 μL of 2.5x SDS sample buffer; then, they were sonicated and boiled for 5 min.

For nuclear fractions, HT22 cells were rinsed twice in ice-cold Tris-buffered saline (TBS), scraped into ice-cold nuclear fractionation buffer (10 mM HEPES pH 7.9, 10 mM KCl, 0.1 mM EDTA, 0.1 mM EGTA, 1 mM DTT, 1 mM Na_3VO_4, 1x protease inhibitor cocktail, and 1x phosphatase inhibitor cocktail), and incubated on ice for 15 min. NP40 at a final concentration of 0.6% was added, and cells were vortexed; the nuclei were pelleted by centrifugation. Nuclear proteins were extracted by sonication of the nuclear pellet in nuclear fractionation buffer, and the extracts were cleared by additional centrifugation. Protein concentrations were quantified by the bicinchoninic acid assay (Pierce, Rockford, IL, USA) and adjusted to equal concentrations. Western blot (5x) sample buffer (74 mM Tris−HCl pH 8.0, 6.25% SDS, 10% β-mercaptoethanol, 20% glycerol) was added to a final concentration of 2.5x, and samples were boiled for 5 min.

Western Blotting. Equal amounts of protein (10−20 μg) per lane were used for SDS−PAGE. All samples were separated using 4−12% Criterion XT Precast Bis−Tris Gels (Biorad, Hercules, CA, USA). Proteins were transferred to nitrocellulose membranes, and the quality of protein measurement, electrophoresis, and transfer were checked by Ponceau S staining. Membranes were blocked with 5% skim milk in TBS-T (20 mM Tris buffer pH 7.5, 0.5 M NaCl, 0.1% Tween 20) for 1 h at room temperature and incubated overnight at 4 °C with the primary antibody diluted in 5% BSA in TBS/0.05% Tween 20. HRP-conjugated rabbit antiactin (#5125, 1/20 000), anti-Nrf2 (#sc-13032, 1/500), antiphospho ERK (#9101, 1/1000), antitotal ERK (#9102, 1/1000), antiphospho p38 (#9212, 1/1000), and antitotal p38 (#9212,1/1000) from Cell Signaling (Danvers, MA, USA) were used as the primary antibody. Subsequently, blots were washed in TBS/

https://dx.doi.org/10.1021/acschemneuro.0c00589
ACS Chem. Neurosci. XXXX, XXX, XXX−XXX

0.05% Tween 20 and incubated for 1 h at room temperature in horseradish peroxidase goat antirabbit or antimouse (Biorad) diluted 1/5000 in 5% skim milk in TBS-T. After additional washing, protein bands were detected by chemiluminescence using the Super Signal West Pico Substrate (Pierce). Autoradiographs were scanned using a Biorad GS800 scanner. Band density was measured using ImageJ. Each Western blot was repeated at least three times with independent protein samples.

CuAAC with Cy3-Azide. Cells (5×10^5 cells per 60 mm dish) were grown overnight, and then the compound or DMSO was added at the indicated concentrations and incubated for 4 h. The CuAAC reaction was performed in a final volume of 120 μL. Therefore, 100 μg of protein were adjusted to the appropriate volume with PBS, and 20 μM Cy3-azide was added followed by freshly prepared tris(2-carboxyethyl)phosphine hydrochloride (TCEP) (1 mM final concentration), tris[(1-benzyl-1H-1,2,3-triazol-4-yl)methylamine (TBTA) (0.1 mM final concentration), and copper sulfate (1 mM final concentration). The mixture was vortexed and incubated rotating at room temperature for 1 h after which the reaction was quenched by the addition of 120 μL of 5X sample buffer. The samples were submitted to SDS−PAGE, transferred to a nitrocellulose membrane, and examined according to the Western blot protocol described above with anti-Cy3 (sc-166894, 1/1000) as a primary antibody.

CuAAC in Fixed Cells for Fluorescence Microscopy. Cells (0.4×10^3 HT22 cells) stably expressing a mitochondria-targeted GFP (mito-GFP) were grown overnight on 24-well plates with coverslips. The next day, compounds were added at the indicated concentrations and incubated for 30 min at 37 °C. After we washed the cells three times for 5 min with warm PBS, the cells were fixed with freshly prepared 4% paraformaldehyde (PFA) in PBS at 37 °C for 20 min and permeabilized with 0.5% Triton X-100 in PBS at room temperature for 15 min. The CuAAC reaction mixture was prepared in an Eppendorf tube by mixing Cy3-azide (20 μM final concentration), freshly prepared tris(2-carboxyethyl)phosphine hydrochloride (TCEP) (1 mM final concentration), tris[(1-benzyl-1H-1,2,3-triazol-4-yl)methylamine (TBTA) (0.1 mM final concentration), and copper sulfate (1 mM final concentration) in PBS. The CuAAC reaction mixture was added to the permeabilized cells and incubated for 1 h at room temperature in the dark. Three additional PBS washing steps were performed before placing the coverslips on slides with mounting media. Images were acquired using a Zeiss LSM 880 Rear Port Laser Scanning Confocal and Airyscan FAST Microscope. GFP and Cy3 were excited sequentially using 488 and 561 laser lines, respectively, and collected using the corresponding filters and the Airyscan detector. The final analysis of the images was performed using ImageJ FIJI software.

CuAAC with HT22 Cells and Affinity Purification of Target Proteins. The procedure was based on Weerapana et al.[60] and Brodziak-Jarosz et al.[21] with modifications. HT22 cells were grown in 10 cm dishes to 90% confluency. Compound **1** (200 μM) or DMSO in fresh medium was added and incubated for 2 h. The cells were washed with ice-cold PBS, scraped into 2 mL of ice-cold PBS, and transferred to Eppendorf tubes. After centrifugation at 5000 rpm for one min, the cells were suspended in 500 μL of lysis buffer (TBS with 1% NP-40, pH 7.4) with protease inhibitor cocktail and left shaking for 20 min at 4 °C. Lysates were centrifuged at 14 000 rpm for 20 min at 4 °C to pellet cellular debris. The supernatant was transferred to fresh Eppendorf tubes, and the protein concentration was determined by the bicinchoninic acid method (Pierce).

The CuAAC reaction was conducted in an Eppendorf tube in a final volume of 500 μL. Protein (2000 μg) was adjusted to the needed volume with PBS and 150 μM Biotin-PEG3-azide (Sigma-Aldrich, Munich, Germany); 1 mM freshly prepared tris(2-carboxyethyl)-phosphine hydrochloride, 0.1 mM tris[(1-benzyl-1H-1,2,3-triazol-4-yl)methylamine, and 1 mM copper sulfate were added. The reaction mixture was vortexed, and then the reaction proceeded for 3 h at room temperature with gentle shaking at which time a precipitate formed. After centrifugation at 6500 *g* for 4 min at 4 °C, the supernatant was collected and immediately submitted to affinity pulldown following the procedure described below. The pellet was washed with 500 μL of ice-cold methanol and sonicated for 4 s, and after 10 min incubation rotating at 4 °C, the suspension was centrifuged at 6500 *g* for 4 min at 4 °C. The supernatant was removed, and the washing step was repeated once. For solubilization, 1 mL of 1.2% SDS in PBS was added to the pellet after the second washing step, and it was sonicated for 4 s and boiled for 5 min when the sample was transferred into a 15 mL falcon tube and diluted with 5 mL PBS to a final SDS concentration of 0.2%. For affinity purification, streptavidin magnetic beads (GE Healthcare) were used according to the manufacturer's protocol with an extended incubation time of 2 h for proteome incubation. After elution in 35 μL of 2.5x sample buffer, a methanol/chloroform extraction was rendered to prepare the samples for MS analysis. The samples were diluted in 140 μL of methanol and 35 μL of chloroform and vortexed. Milli-Q (105 μL) was added, and the mixture was vortexed again before centrifugation at 15 000 rpm for 2 min at 4 °C. The upper layer was removed, and 105 μL of methanol was added and vortexed. After another centrifugation step, the supernatant was removed, and the pellet was left to dry.

MS Analysis. *Gel Electrophoresis.* Precipitated proteins were dissolved in NuPAGE LDS sample buffer (Life Technologies), reduced with 50 mM DTT at 70 °C for 10 min, and alkylated with 120 mM Iodoacetamide at room temperature for 20 min. The separation was performed on NuPAGE Novex 4−12% Bis−Tris gels (Life Technologies) with MOPS buffer according to the manufacturer's instructions. Gels were washed three times for 5 min with water and stained for 1 h with Simply Blue Safe Stain (Life Technologies). After washing with water for 1 h, each gel lane was cut into 14 slices.

In-Gel Digestion. The excised gel bands were destained with 30% acetonitrile in 0.1 M NH_4HCO_3 (pH 8), shrunk with 100% acetonitrile, and dried in a vacuum concentrator (Concentrator 5301, Eppendorf, Germany). Digests were performed with 0.1 μg of trypsin per gel band overnight at 37 °C in 0.1 M NH_4HCO_3 (pH 8). After removing the supernatant, peptides were extracted from the gel slices with 5% formic acid, and extracted peptides were pooled with the supernatant.

NanoLC−MS/MS Analysis. NanoLC−MS/MS analyses were performed on an Orbitrap Fusion (Thermo Scientific) equipped with a PicoView Ion Source (New Objective) and coupled to an EASY-nLC 1000 (Thermo Scientific). Peptides were loaded on capillary columns (PicoFrit, 30 cm × 150 μm ID, New Objective) self-packed with ReproSil-Pur 120 C18-AQ (1.9 μm) (Dr. Maisch) and separated with a 30 min linear gradient from 3 to 30% acetonitrile and 0.1% formic acid and a flow rate of 500 nL/min.

Both MS and MS/MS scans were acquired in the Orbitrap analyzer with a resolution of 60 000 for MS scans and 7500 for MS/MS scans. HCD fragmentation with 35% normalized collision energy was applied. A Top Speed data-dependent MS/MS method with a fixed cycle time of 3 s was used. Dynamic exclusion was applied with a repeat count of 1 and an exclusion duration of 30 s; singly charged precursors were excluded from selection. The minimum signal threshold for precursor selection was set to 50 000. Predictive AGC was used with an AGC target value of 2e5 for MS scans and 5e4 for MS/MS scans. EASY-IC was used for internal calibration.

MS Data Analysis. Raw MS data files were analyzed with MaxQuant version 1.6.2.2.[61] The database search was performed with Andromeda, which is integrated into the utilized version of MaxQuant. The search was performed against the UniProt mouse database. Additionally, a database containing common contaminants was used. The search was performed with tryptic cleavage specificity with 3 allowed miscleavages. Protein identification was under the control of the false-discovery rate (FDR; < 1% FDR on protein and PSM level). In addition to MaxQuant default settings, the search was performed against the following variable modifications: Protein N-terminal acetylation, Gln to pyro-Glu formation (N-term. Gln), and oxidation (Met). Carbamidomethyl (Cys) was set as a fixed modification. Further data analysis was performed using R scripts developed in-house. LFQ intensities were used, and missing LFQ intensities in the control samples were imputed with values close to

https://dx.doi.org/10.1021/acschemneuro.0c00589
ACS Chem. Neurosci. XXXX, XXX, XXX−XXX

the baseline. Data imputation was performed with values from a standard normal distribution with a mean of the 5% quantile of the combined log10-transformed LFQ intensities and a standard deviation of 0.1. For the identification of significantly enriched proteins, mean log2 transformed protein ratios were calculated from the two replicate experiments, and boxplot outliers were identified in intensity bins of at least 300 proteins. Log2 transformed protein ratios of the sample *versus* control with values outside a 1.5x (significance 1) or 3x (significance 2) interquartile range (IQR), respectively, were considered as significantly enriched in the individual replicates. Summed significance values were used to identify best target candidates (significance 2 in both replicates = significance 4). GoTerms were added using Perseus.[62]

Transfection. HT22 cells were plated at 5×10^5 cells per dish in 60 mm tissue culture dishes and grown overnight. The cells were then transfected with 166 pmol siRNA (ANT-1 no. sc-42354; SERCA no. sc-36485, both from Santa Cruz Biotechnology) or control siRNA (no. 1027280; Quiagen) using RNAi max (Invitrogen) according to the manufacturer's instructions. After growth overnight, the cells were subcultured for analysis, as described above.

■ ASSOCIATED CONTENT

Supporting Information

The Supporting Information is available free of charge at https://pubs.acs.org/doi/10.1021/acschemneuro.0c00589.

LC−MS traces and NMR analysis of target compounds **1** and **2** and full list of identified proteins by MS analysis (PDF)

Protein ID and related information (XLSX)

■ AUTHOR INFORMATION

Corresponding Authors

Michael Decker − *Pharmaceutical and Medicinal Chemistry, Institute of Pharmacy and Food Chemistry, Julius Maximilian University of Würzburg, Am Hubland 97074, Würzburg, Germany;* orcid.org/0000-0002-6773-6245; Phone: +49 931 3189676; Email: michael.decker@uni-wuerzburg.de

Pamela Maher − *The Salk Institute for Biological Studies, La Jolla 92037, California, United States of America*; Phone: +1 858 453 4110 1932; Email: pmaher@salk.edu

Authors

Sandra Gunesch − *Pharmaceutical and Medicinal Chemistry, Institute of Pharmacy and Food Chemistry, Julius Maximilian University of Würzburg, Am Hubland 97074, Würzburg, Germany*

David Soriano-Castell − *The Salk Institute for Biological Studies, La Jolla 92037, California, United States of America*

Stephanie Lamer − *Rudolf-Virchow-Zentrum—Center for Integrative and Translational Bioimaging, Julius Maximilian University of Würzburg, 97080 Würzburg, Germany*

Andreas Schlosser − *Rudolf-Virchow-Zentrum—Center for Integrative and Translational Bioimaging, Julius Maximilian University of Würzburg, 97080 Würzburg, Germany*

Complete contact information is available at: https://pubs.acs.org/10.1021/acschemneuro.0c00589

Author Contributions

The manuscript was written through contributions of all authors. All authors have given approval to the final version of the manuscript.

Funding

Financial support by the Bavaria California Technology Center under project number 3 [2018-2] and by the German Academic Exchange Service (DAAD) with funds of the Federal Ministry of Education and Research (BmBF) under project number 57508635 is gratefully acknowledged. P.M. was supported by grants from NIH (RO1 AG046153, RF1 AG054714, and RF1 AG061296).

Notes

The authors declare no competing financial interest.

■ ACKNOWLEDGMENTS

We thankfully acknowledge support by Dr. Antonio Currais (Cellular Biology Laboratory, Salk Institute for Biological Studies) for providing HT22-mitoGFP cells.

■ ABBREVIATIONS

7CT, 7-*O*-cinnamoyltaxifolin; GSH, glutathione; IAA, iodoacetic acid

■ REFERENCES

(1) Patterson, C. *World Alzheimer Report 2018—The State of the Art of Dementia Research: New Frontiers*; Alzheimer's Disease International: London, 2018.

(2) Irvine, G. B., El-Agnaf, O. M., Shankar, G. M., and Walsh, D. M. (2008) Protein aggregation in the brain: the molecular basis for Alzheimer's and Parkinson's diseases. *Mol. Med. 14* (7), 451−464.

(3) Minter, M. R., Taylor, J. M., and Crack, P. J. (2016) The contribution of neuroinflammation to amyloid toxicity in Alzheimer's disease. *J. Neurochem. 136* (3), 457−474.

(4) Simpson, D. S. A., and Oliver, P. L. (2020) ROS Generation in Microglia: Understanding Oxidative Stress and Inflammation in Neurodegenerative Disease. *Antioxidants 9* (743), 1−27.

(5) Ismail, R., Parbo, P., Madsen, L. S., Hansen, A. K., Hansen, K. V., Schaldemose, J. L., Kjeldsen, P. L., Stokholm, M. G., Gottrup, H., Eskildsen, S. F., and Brooks, D. J. (2020) The relationships between neuroinflammation, beta-amyloid and tau deposition in Alzheimer's disease: a longitudinal PET study. *J. Neuroinflammation 17* (1), 151.

(6) Prior, M., Chiruta, C., Currais, A., Goldberg, J., Ramsey, J., Dargusch, R., Maher, P., and Schubert, D. (2014) Back to the future with phenotypic screening. *ACS Chem. Neurosci. 5* (7), 503−513.

(7) Schubert, D., and Maher, P. (2012) An alternative approach to drug discovery for Alzheimer's disease dementia. *Future Med. Chem. 4* (13), 1681−1688.

(8) Pohl, F., and Kong Thoo Lin, P. (2018) The Potential Use of Plant Natural Products and Plant Extracts with Antioxidant Properties for the Prevention/Treatment of Neurodegenerative Diseases: In Vitro, In Vivo and Clinical Trials. *Molecules 23* (12), 3283−3313.

(9) Currais, A., Chiruta, C., Goujon-Svrzic, M., Costa, G., Santos, T., Batista, M. T., Paiva, J., do Ceu Madureira, M., and Maher, P. (2014) Screening and identification of neuroprotective compounds relevant to Alzheimers disease from medicinal plants of S. Tome e Principe. *J. Ethnopharmacol. 155* (1), 830−840.

(10) Maher, P., Fischer, W., Liang, Z., Soriano-Castell, D., Pinto, A. F. M., Rebman, J., and Currais, A. (2020) The Value of Herbarium Collections to the Discovery of Novel Treatments for Alzheimer's Disease, a Case Made With the Genus Eriodictyon. *Front. Pharmacol. 11* (208), 208.

(11) Kling, B., Bücherl, D., Palatzky, P., Matysik, F.-M., Decker, M., Wegener, J., and Heilmann, J. (2014) Flavonoids, Flavonoid Metabolites, and Phenolic Acids Inhibit Oxidative Stress in the Neuronal Cell Line HT-22 Monitored by ECIS and MTT Assay: A Comparative Study. *J. Nat. Prod. 77* (3), 446−454.

(12) Dhakal, S., Kushairi, N., Phan, C. W., Adhikari, B., Sabaratnam, V., and Macreadie, I. (2019) Dietary Polyphenols: A Multifactorial Strategy to Target Alzheimer's Disease. *Int. J. Mol. Sci. 20* (20), 5090.

(13) Maher, P., Akaishi, T., and Abe, K. (2006) Flavonoid fisetin promotes ERK-dependent long-term potentiation and enhances memory. *Proc. Natl. Acad. Sci. U. S. A. 103* (44), 16568−16573.

(14) Inoue, T., Saito, S., Tanaka, M., Yamakage, H., Kusakabe, T., Shimatsu, A., Ihara, M., and Satoh-Asahara, N. (2019) Pleiotropic neuroprotective effects of taxifolin in cerebral amyloid angiopathy. *Proc. Natl. Acad. Sci. U. S. A. 116* (20), 10031−10038.
(15) Schramm, S., Huang, G., Gunesch, S., Lang, F., Roa, J., Hogger, P., Sabate, R., Maher, P., and Decker, M. (2018) Regioselective synthesis of 7-O-esters of the flavonolignan silibinin and SARs lead to compounds with overadditive neuroprotective effects. *Eur. J. Med. Chem. 146* (2018), 93−107.
(16) Vrba, J., Gazak, R., Kuzma, M., Papouskova, B., Vacek, J., Weiszenstein, M., Kren, V., and Ulrichova, J. (2013) A novel semisynthetic flavonoid 7-O-galloyltaxifolin upregulates heme oxygenase-1 in RAW264.7 cells via MAPK/Nrf2 pathway. *J. Med. Chem. 56* (3), 856−866.
(17) Gunesch, S., Hoffmann, M., Kiermeier, C., Fischer, W., Pinto, A. F. M., Maurice, T., Maher, P., and Decker, M. (2020) 7-*O*-esters of taxifolin with pronounced and overadditive effects in neuroprotection, anti-neuroinflammation, and amelioration of short-term memory impairment in vivo. *Redox Biol. 29* (2020), 101378.
(18) Speers, A. E., Adam, G. C., and Cravatt, B. F. (2003) Activity-based protein profiling in vivo using a copper(i)-catalyzed azide-alkyne [3 + 2] cycloaddition. *J. Am. Chem. Soc. 125* (16), 4686−4687.
(19) Bottcher, T., Pitscheider, M., and Sieber, S. A. (2010) Natural products and their biological targets: proteomic and metabolomic labeling strategies. *Angew. Chem., Int. Ed. 49* (15), 2680−2698.
(20) Chen, X., Wong, Y. K., Wang, J., Zhang, J., Lee, Y. M., Shen, H. M., Lin, Q., and Hua, Z. C. (2017) Target identification with quantitative activity based protein profiling (ABPP). *Proteomics 17* (3), 1600212.
(21) Brodziak-Jarosz, L., Fujikawa, Y., Pastor-Flores, D., Kasikci, S., Jirasek, P., Pitzl, S., Owen, R. W., Klika, K. D., Gerhauser, C., Amslinger, S., and Dick, T. P. (2016) A click chemistry approach identifies target proteins of xanthohumol. *Mol. Nutr. Food Res. 60* (4), 737−748.
(22) Nakashima, S., Liu, Z., Yamaguchi, Y., Saiki, S., Munemasa, S., Nakamura, T., Murata, Y., and Nakamura, Y. (2016) A novel tag-free probe for targeting molecules interacting with a flavonoid catabolite. *Biochem. Biophys. Rep. 7* (2016), 240−245.
(23) Su, C., Liu, Z., Wang, Y., Wang, Y., Song, E., and Song, Y. (2017) The electrophilic character of quinones is essential for the suppression of Bach1. *Toxicology 387* (2017), 17−26.
(24) Tan, S., Schubert, D., and Maher, P. (2001) Oxytosis: A novel form of programmed cell death. *Curr. Top. Med. Chem. 1* (6), 497−506.
(25) Currais, A., and Maher, P. (2013) Functional consequences of age-dependent changes in glutathione status in the brain. *Antioxid. Redox Signaling 19* (8), 813−822.
(26) Lewerenz, J., Ates, G., Methner, A., Conrad, M., and Maher, P. (2018) Oxytosis/Ferroptosis-(Re-) Emerging Roles for Oxidative Stress-Dependent Non-apoptotic Cell Death in Diseases of the Central Nervous System. *Front. Neurosci. 12*, 214.
(27) Saxena, U. (2012) Bioenergetics failure in neurodegenerative diseases: back to the future. *Expert Opin. Ther. Targets 16* (4), 351−354.
(28) Schmidlin, C. J., Dodson, M. B., Madhavan, L., and Zhang, D. D. (2019) Redox regulation by NRF2 in aging and disease. *Free Radical Biol. Med. 134* (2019), 702−707.
(29) Bryan, H. K., Olayanju, A., Goldring, C. E., and Park, B. K. (2013) The Nrf2 cell defence pathway: Keap1-dependent and -independent mechanisms of regulation. *Biochem. Pharmacol. 85* (6), 705−717.
(30) Qin, S., and Hou, D. X. (2016) Multiple regulations of Keap1/Nrf2 system by dietary phytochemicals. *Mol. Nutr. Food Res. 60* (8), 1731−1755.
(31) Rai, S. N., Dilnashin, H., Birla, H., Singh, S. S., Zahra, W., Rathore, A. S., Singh, B. K., and Singh, S. P. (2019) The Role of PI3K/Akt and ERK in Neurodegenerative Disorders. *Neurotoxic. Res. 35* (3), 775−795.
(32) Colucci-D'Amato, L., Perrone-Capano, C., and di Porzio, U. (2003) Chronic activation of ERK and neurodegenerative diseases. *BioEssays 25* (11), 1085−1095.
(33) Hensley, K., Floyd, R. A., Zheng, N. Y., Nael, R., Robinson, K. A., Nguyen, X., Pye, Q. N., Stewart, C. A., Geddes, J., Markesbery, W. R., Patel, E., Johnson, G. V., and Bing, G. (1999) p38 kinase is activated in the Alzheimer's disease brain. *J. Neurochem. 72* (5), 2053−2058.
(34) Sun, A., Liu, M., Nguyen, X. V., and Bing, G. (2003) P38 MAP kinase is activated at early stages in Alzheimer's disease brain. *Exp. Neurol. 183* (2), 394−405.
(35) Schnoder, L., Hao, W., Qin, Y., Liu, S., Tomic, I., Liu, X., Fassbender, K., and Liu, Y. (2016) Deficiency of Neuronal p38alpha MAPK Attenuates Amyloid Pathology in Alzheimer Disease Mouse and Cell Models through Facilitating Lysosomal Degradation of BACE1. *J. Biol. Chem. 291* (5), 2067−2079.
(36) Jeong, S. Y., and Seol, D. W. (2008) The role of mitochondria in apoptosis. *BMB reports 41* (1), 11−22.
(37) Jeong, S. (2017) Molecular and Cellular Basis of Neurodegeneration in Alzheimer's Disease. *Mol. Cells 40* (9), 613−620.
(38) Gao, M., Yi, J., Zhu, J., Minikes, A. M., Monian, P., Thompson, C. B., and Jiang, X. (2019) Role of Mitochondria in Ferroptosis. *Mol. Cell 73* (2), 354−363.
(39) Krainz, T., Gaschler, M. M., Lim, C., Sacher, J. R., Stockwell, B. R., and Wipf, P. (2016) A Mitochondrial-Targeted Nitroxide Is a Potent Inhibitor of Ferroptosis. *ACS Cent. Sci. 2* (9), 653−659.
(40) Neitemeier, S., Jelinek, A., Laino, V., Hoffmann, L., Eisenbach, I., Eying, R., Ganjam, G. K., Dolga, A. M., Oppermann, S., and Culmsee, C. (2017) BID links ferroptosis to mitochondrial cell death pathways. *Redox Biol. 12* (2017), 558−570.
(41) Basit, F., van Oppen, L. M., Schockel, L., Bossenbroek, H. M., van Emst-de Vries, S. E., Hermeling, J. C., Grefte, S., Kopitz, C., Heroult, M., HGM Willems, P., and Koopman, W. J. (2017) Mitochondrial complex I inhibition triggers a mitophagy-dependent ROS increase leading to necroptosis and ferroptosis in melanoma cells. *Cell Death Dis. 8* (3), No. e2716.
(42) Huff, J. (2015) The airyscan detector form ZEISS: confocal imaging with improved signal-to-noise ratio and super-resolution. *Nat. Methods 12*, 1−2.
(43) Brand, M. D., Pakay, J. L., Ocloo, A., Kokoszka, J., Wallace, D. C., Brookes, P. S., and Cornwall, E. J. (2005) The basal proton conductance of mitochondria depends on adenine nucleotide translocase content. *Biochem. J. 392* (2), 353−362.
(44) Liu, Y., and Chen, X. J. (2013) Adenine Nucleotide Translocase, Mitochondrial Stress, and Degenerative Cell Death. *Oxid. Med. Cell. Longevity 146860*, 1−10.
(45) Chevrollier, A., Loiseau, D., Reynier, P., and Stepien, G. (2011) Adenine nucleotide translocase 2 is a key mitochondrial protein in cancer metabolism. *Biochim. Biophys. Acta, Bioenerg. 1807* (6), 562−567.
(46) Ruprecht, J. J., King, M. S., Zögg, T., Aleksandrova, A. A., Pardon, E., Crichton, P. G., Steyaert, J., and Kunji, E. R. S. (2019) The Molecular Mechanism of Transport by the Mitochondrial ADP/ATP Carrier. *Cell 176* (3), 435−447.
(47) Wang, W., Zhao, F., Ma, X., Perry, G., and Zhu, X. (2020) Mitochondria dysfunction in the pathogenesis of Alzheimer's disease: recent advances. *Mol. Neurodegener. 15* (30), 1−22.
(48) Cadonic, C., Sabbir, M. G., and Albensi, B. C. (2016) Mechanisms of Mitochondrial Dysfunction in Alzheimer's Disease. *Mol. Neurobiol. 53* (9), 6078−6090.
(49) Bobba, A., Amadoro, G., Azzariti, A., Pizzuto, R., and Atlante, A. (2014) Extracellular ADP prevents neuronal apoptosis via activation of cell antioxidant enzymes and protection of mitochondrial ANT-1. *Biochim. Biophys. Acta, Bioenerg. 1837* (8), 1338−1349.
(50) Bauer, M. K., Schubert, A., Rocks, O., and Grimm, S. (1999) Adenine nucleotide translocase-1, a component of the permeability transition pore, can dominantly induce apoptosis. *J. Cell Biol. 147* (7), 1493−1502.

https://dx.doi.org/10.1021/acschemneuro.0c00589
ACS Chem. Neurosci. XXXX, XXX, XXX−XXX

(51) Liu, Y., and Schubert, D. (2009) The specificity of neuroprotection by antioxidants. *J. Biomed. Sci. 16* (98), 1−14.
(52) Tan, S., Sagara, Y., Liu, Y., Maher, P., and Schubert, D. (1998) The regulation of reactive oxygen species production during programmed cell death. *J. Cell Biol. 141* (6), 1423−1432.
(53) Ortega, R., and García, N. (2009) The flavonoid quercetin induces changes in mitochondrial permeability by inhibiting adenine nucleotide translocase. *J. Bioenerg. Biomembr. 41* (1), 41−47.
(54) Appleby, R. D., Porteous, W. K., Hughes, G., James, A. M., Shannon, D., Wei, Y. H., and Murphy, M. P. (1999) Quantitation and origin of the mitochondrial membrane potential in human cells lacking mitochondrial DNA. *Eur. J. Biochem. 262* (1), 108−116.
(55) Zorova, L. D., Popkov, V. A., Plotnikov, E. Y., Silachev, D. N., Pevzner, I. B., Jankauskas, S. S., Babenko, V. A., Zorov, S. D., Balakireva, A. V., Juhaszova, M., Sollott, S. J., and Zorov, D. B. (2018) Mitochondrial membrane potential. *Anal. Biochem. 552* (2018), 50−59.
(56) Ren, R., Zhang, Y., Li, B., Wu, Y., and Li, B. (2011) Effect of β-amyloid (25−35) on mitochondrial function and expression of mitochondrial permeability transition pore proteins in rat hippocampal neurons. *J. Cell. Biochem. 112* (5), 1450−1457.
(57) Song, X. B., Liu, G., Wang, Z. Y., and Wang, L. (2016) Puerarin protects against cadmium-induced proximal tubular cell apoptosis by restoring mitochondrial function. *Chem.-Biol. Interact. 260* (2016), 219−231.
(58) Unterberger, U., Höftberger, R., Gelpi, E., Flicker, H., Budka, H., and Voigtländer, T. (2006) Endoplasmic reticulum stress features are prominent in Alzheimer disease but not in prion diseases in vivo. *J. Neuropathol. Exp. Neurol. 65* (4), 348−357.
(59) Krajnak, K., and Dahl, R. (2018) A new target for Alzheimer's disease: A small molecule SERCA activator is neuroprotective in vitro and improves memory and cognition in APP/PS1 mice. *Bioorg. Med. Chem. Lett. 28* (9), 1591−1594.
(60) Weerapana, E., Speers, A. E., and Cravatt, B. F. (2007) Tandem orthogonal proteolysis-activity-based protein profiling (TOP-ABPP)—a general method for mapping sites of probe modification in proteomes. *Nat. Protoc. 2* (6), 1414−1425.
(61) Cox, J., and Mann, M. (2008) MaxQuant enables high peptide identification rates, individualized p.p.b.-range mass accuracies and proteome-wide protein quantification. *Nat. Biotechnol. 26* (12), 1367−1372.
(62) Tyanova, S., Temu, T., Sinitcyn, P., Carlson, A., Hein, M. Y., Geiger, T., Mann, M., and Cox, J. (2016) The Perseus computational platform for comprehensive analysis of (prote)omics data. *Nat. Methods 13* (9), 731−740.

https://dx.doi.org/10.1021/acschemneuro.0c00589
ACS Chem. Neurosci. XXXX, XXX, XXX−XXX